Singularity Analysis of Rigid Directed Bearing Graphs for Quadrotor Formations

Julian Erskine, Sébastien Briot, Isabelle Fantoni, and Abdelhamid Chriette

***Abstract*—The decentralization of formations using onboard sensing is important for multirobot systems, improving the robustness and independence of fleet operations. Bearing measurements (obtainable from embedded cameras) are an attractive choice for use in decentralized formation control, however, this requires that the formation framework be bearing rigid. Rigidity may be checked numerically for a given formation framework, however, it remains difficult to determine the geometric conditions under which otherwise rigid formations become flexible. This article models the sensor and robot constraints in bearing formations of quadrotors as a kinematic mechanism with analogous properties to find geometric conditions for the degeneration of bearing rigidity (singularities) and the resulting uncontrollable motions. A classification of singularities based on graph substructures is developed, and it is shown that arbitrarily large formations may be designed for which all singularities lie within a known set of geometric conditions. An application on how to use the knowledge of all singularity cases in a formation for singularity-free control maintenance is provided.**

***Index Terms*—Bearing formations, graph rigidity, kinematics, multirobot systems, sensor-based control.**

I. Introduction

UNMANNED aerial vehicles (UAVs) are playing increasingly large roles in many sectors, such as search and rescue, surveillance, imaging, transportation, and entertainment [1], [2], [3], [4], [5]. While UAVs with omni-directional actuation on the SE(3) manifold are emerging (primarily for aerial manipulation tasks) [6], [7], [8], [9], quadrotor-style UAVs, which are differentially flat on the $\mathbb{R}^3 \times \mathcal{S}^1$ manifold are much more common due to their greater energy efficiency and mechanical simplicity while benefiting from vertical takeoff and landing capabilities. This article deals explicitly with the later UAVs, however, it may be applied to any group of robots that are differentially flat on the $\mathbb{R}^3 \times \mathcal{S}^1$ or SE(2) manifolds (or other submanifolds), which include many mobile robots.

The usefullness of UAVs is frequently limited by their autonomy and sensing capabilities, however, these constraints may be mitigated by using teams of robots [10], [11], [12]. These may use a swarming behavior when the objective is to control the aggregate motion of a large number of robots [13], [14], or formation control when a *prescribed inter-robot geometry* is desired. The latter is useful when multiple specific viewing angles, enforced lines of sight, guaranteed, or optimized area coverage or other geometrically defined mission parameters are required. This can be achieved with a centralized controller if there is reliable robot positioning in a common frame, however, centralized control scales poorly with the number of robots. Furthermore, it is often desireable for the robots to use information from only onboard sensors, increasing the formations robustness to external sensor failures or communication disturbances [15], [16], [17]. Decentralized (or distributed) control in which each agent performs its cooperative task using local sensing and computing is, thus, seen as an interesting alternative. Monocular cameras (bearing sensors) are of great interest for decentralized formation control as they are cheap, light, energy efficient, and are often already incorporated for other purposes, however, they suffer from a difficulty in estimating the interagent depth. Other sensors, such as lidars, RGB-D cameras, or stereo vision systems can be used to measure relative inter-robot positions, but their higher cost, weight (a critical factor in aerial robotics), and computational requirements detract from their attractiveness.

Extensive work has already been devoted to the formation control problem (and the analogous network localization problem, thus, we may use the term "Agent" for increased generality compared to the term "Robot," see [18]) using onboard sensors. Initial work considered planar agents with interagent distances [19], [20], [21] or bearing [22], [23], [24], [25], [26] measurements. It was remarked by the community that the rigidity of the sensing graph is critical to the finite-time convergence of gradient-based formation controllers [27], [28], and necessary for the agents to be capable of reconstructing a geometry given the interagent measurements. Work on formation control has been applied specifically to the $\mathbb{R}^3 \times \mathcal{S}^1$ manifold for quadrotor fleets, and often using the notion of rigidity from algebraic graph theory [29], [30], [31]. Certain controllers have been designed to maintain rigidity in formations [32], [33], however, they use externally calculated global characteristics of the formation and are, thus, not fully decentralized. Other work deals with the

Manuscript received 6 March 2023; revised 18 July 2023; accepted 4 October 2023. Date of publication 16 October 2023; date of current version 15 December 2023. This paper was recommended for publication by Associate Editor R. Tron and Editor P. Robuffo Giordano upon evaluation of the reviewers' comments. This work was supported in part by the French region Pays de la Loire through the RFI AtlanSTIC2020 project RAPID and in part by the Natural Sciences and Engineering Research Council of Canada. *(Corresponding author: Sébastien Briot.)*

Julian Erskine and Abdelhamid Chriette are with the École Centrale de Nantes, Laboratoire des Sciences du Numèrique de Nantes, 44321 Nantes, France (e-mail: julian.erskine@ls2n.fr; adbelhamid.chriette@ls2n.fr).

Sébastien Briot and Isabelle Fantoni are with the Centre National de la Recherche Scientifique, Laboratoire des Sciences du Numèrique de Nantes, 44321 Nantes, France (e-mail: sebastien.briot@ls2n.fr; isabelle.fantoni@ls2n.fr).

This article has supplementary material provided by the authors and color versions of one or more figures available at https://doi.org/10.1109/TRO.2023.3324198.

Digital Object Identifier 10.1109/TRO.2023.3324198

IEEE Transactions on Robotics (T-RO) paper, presented at ICRA 2024, Yokohama, Japan. Cite as T-RO paper.

creation of rigid graphs given a set of agent positions [34]. In [35], [36], and [34], algorithms for building or identifying generic bearing rigid graphs in $\mathbb{R}^n$ were discussed, while approaches for restoring bearing rigidity are presented in [34] and [37]. However, few analyze the geometric conditions for which the rigidity of a given bearing graph may be lost.

Formations can be analyzed and designed in a combinatorial approach using graph theory. Tools, such as Henneburg graph construction [28], [38], [39], can ensure *generic rigidity*, which means that the graph is almost always rigid. In [40], it is recognized that some embeddings of the same graph may display different rigidity properties, and that a graph is either rigid for "almost all" embeddings or flexible for "almost all" embeddings. This work deals with the complement of "almost all," called singular configurations, where the rigidity is locally lost, introducing one or more additional degrees of freedom (DOF) into the formation. Indeed, singular configurations are not unlikely despite being a very small subset of all configurations. As shown in [41] and further on in this article, they may occur in formations of regular geometries, such as all agents belonging to a common horizontal plane, or to the vertices of common regular polyhedrons. While rigidity in the graph theory sense is a mature subject with applications in network localization, CAD software, civil engineering, and many others [40], [42], [43], [44], to the best of authors' knowledge, the singularities of bearing graphs have never been generally and systematically studied, even in recent and otherwise complete works on bearing rigidity theory for multiagent systems, such as [16], [45].

Recognizing the link between rigid formations and visual servoing, a technique used in the latter to facilitate the identification of singular configurations was recently extended to the analysis of bearing graphs [41]. It was shown that the sensing and actuation of the agents may be replaced by an analogous set of kinematic constraints, known as a "virtual mechanism" or "hidden robot." This allowed the wealth of existing literature in the field of robot kinematics and parallel mechanisms to be applied to the analysis of singular formation configurations. Nonetheless, a direct application of this tool is not easily scaled beyond the analysis of small formations of 3–4 agents, and requires a complex individual analysis of each new formation being studied. Indeed, even for small formations, it may be difficult to apply for users not well practiced in the analysis of parallel kinematic mechanisms. As formation singularities are primarily of interest to the multiagent control community for whom the required tools for this analysis are little used, the direct applicability of [41] is limited. Nonetheless it provides an interesting base from which to develop a general geometric analysis of rigid bearing graph singularities.

What we propose in this article is a methodology based on the virtual mechanism concept that simplifies the geometric identification of singularities in bearing formations of quadrotors. Analyzing simple substructures of directed graphs, singularities are classified based on the graph structure, which in many cases eliminates the need for an ad hoc analysis of the entire virtual mechanism of a given formation. While we do not claim to be capable of detecting all singular configurations of all possible formations (there is currently no universal method for singularity detection), our work permits the design of arbitrarily large formation graphs with completely identified sets of singularities, which has potential for use in rigidity maintenance to guarantee controller performance.

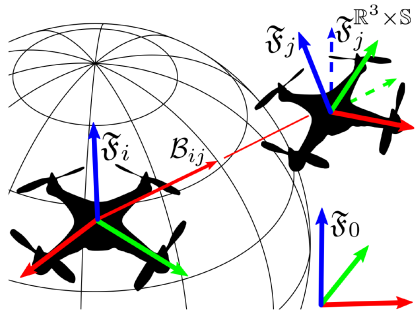

Fig. 1. Bearing measurement of quadrotor j by quadrotor i. This article considers that all states and measurements are reprojected onto the $\mathbb{R}^3 \times \mathcal{S}^1$ manifold (see the dashed frame axes of quadrotor j).

The rest of this article is organized as follows. Section II presents the modeling and assumptions classically used for the agent and formation dynamics and Section III recalls the tools needed to analyze the rigidity of formations (e.g., screw theory and the principle of the virtual mechanism). Section IV introduces the classification strategy for different graph substructure types, and the corresponding singularity classes are presented in Sections V and VI. Section VII presents how our method can be applied to design formations with fully known sets of singularities and shows that this is scaleable for very large formations. It also highlights in a case study how the knowledge of all singularity cases in a formation can be used in order to perform singularity-free-maintenance control. Finally, Section VIII concludes this article.

II. Modeling

A. Review on Agent Modeling

The agents here are considered as quadrotor-style UAVs moving on an $\mathbb{R}^3 \times \mathcal{S}^1$ manifold with respect to a fixed frame $\mathfrak{F}_0 = \{O_0, \mathbf{x}_0, \mathbf{y}_0, \mathbf{z}_0\}$ of origin O_0. The $\mathbb{R}^3$ component is the 3-D Cartesian space spanned by $\mathbf{x}_0, \mathbf{y}_0$, and $\mathbf{z}_0$, while $\mathcal{S}^1$ represents the rotational space around $\mathbf{z_0}$. Each agent $\mathcal{A}_i$ has an associated frame $\mathfrak{F}_i = \{O_i, \mathbf{x}_i, \mathbf{y}_i, \mathbf{z}_i\}$ with O_i at the geometric centre of the quadrotor and $\mathbf{z}_i$ being parallel to the axis of the propellers, as shown in Fig. 1. The translation of $\mathfrak{F}_i$ with relative to $\mathfrak{F}_0$ and expressed in $\mathfrak{F}_0$ is $\mathbf{p}_i$, and its rotation with respect to $\mathfrak{F}_0$ is expressed by the rotation matrix $\mathbf{R}_i$. Quadrotors have well-known coupling between their roll and pitch and their horizontal translational dynamics due to their underactuation, but their roll and pitch are necessarily well estimated from onboard sensors for stable flight. All measurements in $\mathfrak{F}_i$ (which in reality evolves on $\mathrm{SE}(3)$) can, therefore, be reprojected onto a flat frame on the $\mathbb{R}^3 \times \mathcal{S}^1$ manifold for which the rotation matrix $\mathbf{R}_i$ is only a function of the yaw rotation ψ_i around $\mathbf{z}_0$, such that $\mathbf{z}_i = \mathbf{z}_0$. The state $\mathbf{q}_i = [\mathbf{p}_i^T \ \psi_i]^T$ can, therefore, be chosen as the flat outputs of the quadrotor in $\mathfrak{F}_0$. The agent may be controlled using its body frame velocity (or acceleration),

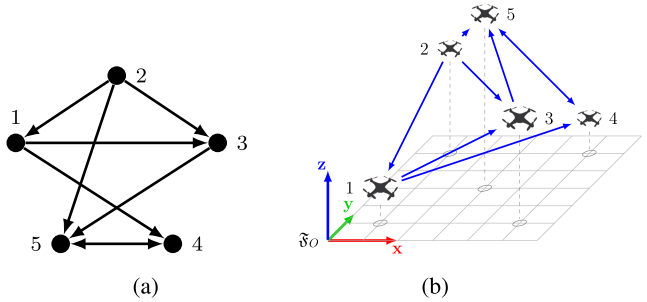

Fig. 2. Graph and framework representations of a directed bearing formation. (a) Directed graph, showing the flow of information between nodes. (b) Embedding of (a) in $\mathbb{R}^3 \times \mathcal{S}^1$, where each node i has an associated state $\mathbf{q}_i = [\mathbf{p}_i \in \mathbb{R}^3, \psi_i \in \mathcal{S}^1]$.

thus, the state evolves as $\dot{\mathbf{q}}_i = [(\mathbf{R}_i \mathbf{v}_i)^T \ \dot{\psi}_i]^T$ where $\mathbf{v}_i \in \mathbb{R}^3$ and $\dot{\psi}_i \in \mathcal{S}^1$ are the linear velocities and yaw rate of $\mathcal{A}_i$ in $\mathfrak{F}_i$.

For the purposes of bearing formation control, we assume that each agent is able to detect the bearings of certain other agents in its own frame, which may be easily extracted from a monocular camera or other bearing sensor [46]. The bearing $\boldsymbol{\beta}_{ij}$ of $\mathcal{A}_j$ observed by $\mathcal{A}_i$ in $\mathfrak{F}_i$ is given by

$$\boldsymbol{\beta}_{ij} = \mathbf{R}_i^T \frac{\mathbf{p}_{ij}}{d_{ij}} \in \mathcal{S}^2 \tag{1}$$

where $\mathbf{p}_{ij} = \mathbf{p}_j - \mathbf{p}_i$ and $d_{ij} = ||\mathbf{p}_j - \mathbf{p}_i||$. It corresponds to the relative direction between the two agents in the frame of the observing agent $\mathcal{A}_i$, projected onto a unit sphere about $\mathfrak{F}_i$, as shown in Fig. 1.

B. Recalls on Formation Modeling

Bearing formations in multiagent control are often expressed as directed graphs $\mathcal{G} = (\mathcal{V}, \mathcal{E})$, where each agent $\mathcal{A}_i$ is represented by a vertex $\mathcal{V}_i \in \mathcal{V}$, and each measurement $\boldsymbol{\beta}_{ij}$ by an edge $\mathcal{E}_{ij} = \mathcal{V}_i \times \mathcal{V}_j \in \mathcal{E}$ such that $\mathcal{V}_i, \mathcal{V}_j \in \mathcal{V}$ and $i \neq j$ (see the example on Fig. 2). The formation bearing vector $\boldsymbol{\beta}(\mathbf{q}) = [\boldsymbol{\beta}_{\mathcal{E}_1}^T \ldots \boldsymbol{\beta}_{\mathcal{E}_{|\mathcal{E}|}}^T]^T$ is the stacked vector of all bearings, and the formation state vector $\mathbf{q} = [\mathbf{q}_1^T \ldots \mathbf{q}_{|\mathcal{V}|}^T]^T$ is the stacked vector of all agents' states, where $|\mathcal{V}|$ and $|\mathcal{E}|$ are the number of vertices and directed edges, respectively [47].

A framework $\mathcal{F}(\mathcal{G}, \ \mathbf{q})$ extends the combinatoric information of the graph by an embedding $\mathbf{q} = [\mathbf{q}_1^T \cdots \mathbf{q}_{|\mathcal{V}|}^T]^T$, such that each vertex $\mathcal{V}_i$ is associated with a corresponding state $\mathbf{q}_i = [\mathbf{p}_i \ \psi_i]^T$ of $\mathcal{A}_i$. The bearing formation control problem attempts to drive the formation to a desired framework defined by a desired bearing vector $\boldsymbol{\beta}^d$, possibly with additional tasks, such as controlling the formation scale or the position of the formation [48]. This is often done through the kinematic model

$$\dot{\boldsymbol{\beta}} = \mathbf{B}\dot{\mathbf{q}} \tag{2}$$

where $\mathbf{B} = \frac{\partial \boldsymbol{\beta}(\mathbf{q})}{\partial \mathbf{q}} \in \mathbb{R}^{3|\mathcal{E}| \times 4|\mathcal{V}|}$ is the bearing rigidity matrix, which can be constructed from $\mathcal{F}$, as shown in [29]. As shown in this work, the kth row block of the bearing rigidity matrix $\mathbf{B}$ associated to an edge $\mathcal{E}_k = \mathcal{V}_i \times \mathcal{V}_j$ is given by the expression

$$\mathbf{B}_k = \left[\mathbf{-0-} \ \underbrace{-\frac{\mathbf{P}_{ij}\mathbf{R}_i^T}{d_{ij}}}_{4i-3:4i-1} \ \underbrace{-\mathbf{S}\boldsymbol{\beta}_{ij}}_{4i} \ \mathbf{-0-} \ \underbrace{\frac{\mathbf{P}_{ij}\mathbf{R}_i^T}{d_{ij}}}_{4j-3:4j-1} \ \mathbf{-0-} \right] \tag{3}$$

where $\mathbf{B}_k \in \mathbb{R}^{3 \times 4|\mathcal{V}|}$ relates $\dot{\boldsymbol{\beta}}_{ij}$ to $\dot{\mathbf{q}}$ by

$$\dot{\boldsymbol{\beta}}_{ij} = \mathbf{B}_k \dot{\mathbf{q}} \tag{4}$$

such that the columns $4i-1$ to $4i$ ($4j-1$ to $4j$, resp.) of $\mathbf{B}_k$ are multiplied by the drone $\mathcal{A}_i$ velocity vector $\dot{\mathbf{q}}_i$ (the drone $\mathcal{A}_j$ velocity vector $\dot{\mathbf{q}}_j$, resp.). Moreover, $\mathbf{P}_{ij} = \mathbf{I}_3 - \boldsymbol{\beta}_{ij}\boldsymbol{\beta}_{ij}^T$ is the orthogonal projector onto the orthogonal complement of $\boldsymbol{\beta}_{ij}$, and $\mathbf{S} = \left[[0 \ 0 \ 1]^T\right]_\times$ where $\left[.\right]_\times$ indicates the usual skew-symmetric matrix operator.

$\mathcal{F}$ is said to be bearing rigid (we only consider infinitessimal bearing rigidity in this article, other types of bearing rigidity are implied by it [16]) if the embedding $\mathbf{q}$ may be uniquely determined from $\boldsymbol{\beta}$ up to a common set of trivial motions $\mathfrak{M}$ (i.e., motions of the embedding of the formation preserving bearing congruency) [45]. For bearing formations in $\mathbb{R}^3 \times \mathcal{S}^1$ it is proven that $\mathfrak{M} = [\mathbf{v}_\mathcal{F}, \psi_\mathcal{F}, \dot{s}_\mathcal{F}]$ consists of a coordinated translation $\mathbf{v}_\mathcal{F} \in \mathbb{R}^3$ of the formation, a rotation $\dot{\psi}_\mathcal{F} \in \mathcal{S}^1$ of the formation around an axis parallel to $\mathbf{z}_0$, and a uniform expansion $\dot{s}_\mathcal{F} \in \mathbb{R}^1$ of the formation about any common point [29]. Let us denote as $\mathbf{V}_\mathfrak{M}$ a matrix representing all possible motions for each of the drones belonging to $\mathfrak{M}$. This matrix is always in the kernel of the bearing rigidity matrix

$$\mathbf{V}_\mathfrak{M} \in \ker(\mathbf{B}) \tag{5}$$

and as such have no impact on $\boldsymbol{\beta}$. Let us denote as $\mathcal{N}_B$ a matrix spanning the nullspace of $\mathbf{B}$. If rank $(\mathcal{N}_B) >$ rank $(\mathbf{V}_\mathfrak{M})$, then there exists rank $(\mathcal{N}_B) -$ rank $(\mathbf{V}_\mathfrak{M})$ DOF internal to the formation. In this case, the framework of a formation defined by the bearings of a desired framework $\boldsymbol{\beta}^d = f(\mathcal{F}^d(\mathcal{G}, \mathbf{q}^d))$ will not necessary be congruent to $\mathcal{F}^d$. If rank $(\mathcal{N}_B) =$ rank $(\mathbf{V}_\mathfrak{M})$, then the formation is bearing rigid, otherwise it is flexible.

To verify if a given bearing graph is generically rigid on $\mathbb{R}^3 \times \mathcal{S}^1$, it is sufficient to check that rank $(\mathcal{N}_B) = 5$ (with $\mathbf{B}$ being built from any random embedding) [29], otherwise the framework is generically flexible and the graph is not of interest in bearing formation control as it will never be rigid. Once $\mathcal{F}$ is shown to be generically rigid, however, some special (singular) embeddings may result in a roto-flexible framework for which agents can move outside of $\mathfrak{M}$ (i.e., $\mathcal{N}_B$ gains rank) and, thus, we cannot enforce congruence between the formations with the same set of measurements. Finding the geometric criteria for these singular configurations, and a geometric interpretation of their effect is the objective of this article.

III. Screw Theory and Virtual Mechanisms

Until recently, singular formation states were identified primarily through intuition (such as the case when three agents are aligned) or by an evaluation of the eigenvalues of the rigidity matrix [49]. The latter fails to give a physical interpretation of

the singular motion and cannot be used to globally map the singularity locii of large formations, however, it is useful if the goal is to assess the rigidity for a few specific formation embeddings. In [41], the "hidden robot" concept, initially developed for the study of singularities in visual servoing, was extended to the singularity analysis of bearing-rigidity in multiagent formation control. This concept permits the identification of a virtual closed-loop mechanical architecture with the same singularity properties as the bearing-rigid formation. Then, the tools for singularity analysis developed in the parallel robotics community, such as screw theory allow for the analysis of singular formation configurations. In this section, we make some recalls on screw theory and on the concept of the hidden robot, and develop notation necessary for the following of this article.

A. Recall of Screw Theory

Screw theory will be used further on to analyze the mobility of formations, and is briefly recalled here. The reader is referred to [50] for the theoretical basis of screw theory and to [51] for more practical applications in mechanics. A generalized screw $\$$ is a mathematical feature that can be represented by a vector with six components taking the following expression:

$$\$ = \begin{bmatrix} \mathbf{s} \\ \mathbf{s} \times \mathbf{p} + \lambda \mathbf{s} \end{bmatrix} \tag{6}$$

where $\mathbf{s}$ is a three-component vector called the axis of the screw, λ is a scalar value called the pitch and $\mathbf{p}$ is the location of P, a point of application. If the pitch λ is equal to zero, then

$$\$^0 = \begin{bmatrix} \mathbf{s} \\ \mathbf{s} \times \mathbf{p} \end{bmatrix} \tag{7}$$

and the screw $\$^0$ is called a zero-pitch screw. If the pitch λ is infinite, then the screw is defined such that

$$\$^\infty = \begin{bmatrix} \mathbf{0} \\ \mathbf{s} \end{bmatrix} \tag{8}$$

and the screw $\$^\infty$ is called a infinite-pitch screw. While other screw pitches exist, all screws in our application may be decomposed into a combination of zero and infinite pitch screws, therefore, only these are treated.

The screw notation is used to represent velocity twists $\mathbb{v}$ (consisting of angular $\boldsymbol{\omega}$ and translational $\mathbf{v}$ velocities) and wrenches $\mathbb{w}$ (consisting of forces $\mathbf{f}$ and moments $\mathbf{m}$)

$$\mathbb{v} = \begin{bmatrix} \boldsymbol{\omega} \\ \mathbf{v} \end{bmatrix} \quad \mathbb{w} = \begin{bmatrix} \mathbf{f} \\ \mathbf{m} \end{bmatrix}. \tag{9}$$

A zero-pitch twist $\mathbb{v}^{\mathrm{r}}(\mathbf{s}, \mathbf{p})$ represents a pure infinitesimal rotation with a scalar angular velocity ω around an axis $\mathbf{s}$ at point $\mathbf{p}$, and an infinite-pitch twist $\mathbb{v}^{\mathrm{t}}(\mathbf{s})$ represents a pure infinitesimal translation with velocity v along axis $\mathbf{s}$

$$\mathbb{v}^{\mathrm{r}} = \begin{bmatrix} \omega \mathbf{s} \\ \omega \mathbf{s} \times \mathbf{p} \end{bmatrix} \quad \mathbb{v}^{\mathrm{t}} = \begin{bmatrix} \mathbf{0} \\ v \mathbf{s} \end{bmatrix}. \tag{10}$$

Applied to quadrotor i operating on the $\mathbb{R}^3 \times \mathcal{S}^1$ manifold, the twists can be parameterized based on the state derivative $\dot{\mathbf{q}}_i$ and the point of interest $\mathbf{p}$

$$\mathbb{v}_i^{\mathrm{r}} = \begin{bmatrix} \dot{\psi}_i \mathbf{z}_0 \\ \dot{\psi}_i \mathbf{z}_0 \times \mathbf{p} \end{bmatrix} \quad \mathbb{v}_i^{\mathrm{t}} = \begin{bmatrix} \mathbf{0} \\ \mathbf{v}_i \end{bmatrix}. \tag{11}$$

Two wrench types can be represented similar to the twists. A zero-pitch wrench $\mathbb{w}^{\mathrm{f}}(\mathbf{s}, \mathbf{p})$ represents a pure force f along axis $\mathbf{s}$ acting at position $\mathbf{p}$ with respect to some frame of reference, and an infinite-pitch wrench $\mathbb{w}^{\mathrm{m}}(\mathbf{s})$ represents a pure moment m around axis $\mathbf{s}$ [51]

$$\mathbb{w}^{\mathrm{f}} = \begin{bmatrix} f \mathbf{s} \\ f \mathbf{s} \times \mathbf{p} \end{bmatrix} \quad \mathbb{w}^{\mathrm{m}} = \begin{bmatrix} \mathbf{0} \\ m \mathbf{s} \end{bmatrix}. \tag{12}$$

Twists and wrenches are usually used in order to characterize the kinetostatic behavior of bodies and/or mechanisms. For a body (or a mechanism) having n DOF ($n \leq 6$), it is possible to define a set of n linearly independent twists $\mathcal{T} = \{\mathbb{v}_1 \ldots \mathbb{v}_n\}$ spanning the basis of the feasible velocities for the kinematic chain [52] (assuming no kinematic redundancy). As a result, there is necessarily a wrench set $\mathcal{W} = \{\mathbb{w}_1 \ldots \mathbb{w}_{6-n}\}$ containing $6 - n$ wrenches defined such that they produce no infinitesimal power if applied to the mechanism, i.e., any wrench $\mathbb{w}$ belonging to $\mathcal{W}$ must satisfy the condition

$$\mathbb{v} \circ \mathbb{w} = 0 \quad \forall \mathbb{v} \in \mathcal{T} \quad \forall \mathbb{w} \in \mathcal{W} \tag{13}$$

where the reciprocal product (denoted by the $\circ$ operator) of two screws $\$_1$ and $\$_2$ is defined by

$$\$_1 \circ \$_2 = \left(\begin{bmatrix} \mathbf{0} & \mathbf{I}_3 \\ \mathbf{I}_3 & \mathbf{0} \end{bmatrix} \$_1 \right)^T \$_2. \tag{14}$$

The reciprocity conditions of screws are well studied [51], and for the types of screws used in this article, they can be summarized as, for twists $\mathbb{v}_A^{\mathrm{t}}$ and wrenches $\mathbb{w}_B^{\mathrm{f}}$:

1) $\mathbb{v}_A^{\mathrm{t}} \circ \mathbb{w}_B^{\mathrm{f}} = 0$ if $\mathbf{s}_A$ and $\mathbf{s}_B$ are orthogonal;
2) $\mathbb{v}_A^{\mathrm{t}} \circ \mathbb{w}_B^{\mathrm{m}} = 0$ for all $\mathbb{v}^{\mathrm{t}}$ and $\mathbb{w}^{\mathrm{m}}$;
3) $\mathbb{v}_A^{\mathrm{r}} \circ \mathbb{w}_B^{\mathrm{f}} = 0$ if Plücker lines[1] of coordinates $\mathbb{v}_A^{\mathrm{r}}$ and $\mathbb{w}_B^{\mathrm{f}}$ intersect;
4) $\mathbb{v}_A^{\mathrm{r}} \circ \mathbb{w}_B^{\mathrm{m}} = 0$ if $\mathbf{s}_A$ and $\mathbf{s}_B$ are orthogonal.

Note that other reciprocity conditions involving finite pitch screws could be defined but are not useful for what follows. Therefore, we do not display them.

An example of application of this theory for the computation of the twist and wrench sets of an RR serial chain is provided in the Appendix.

It was shown in [41] that the singularities of formations appear when the wrench set associated with a virtual closed-loop mechanism degenerates, i.e., becomes singular. This mechanism can be found thanks to the "hidden robot" concept, and has the same kinematic properties as the studied formation (see

[1] A Plücker line is a redundant representation of a line [53]. For a line passing through two points A and B, it uses the line direction $\mathbf{u} = \overrightarrow{AB}$ and the moment $\mathbf{h} = \overrightarrow{MA} \times \mathbf{u} = \overrightarrow{MB} \times \mathbf{u}$ of $\mathbf{u}$ about a point M whose position is known in the space. Plücker lines could be used to represent zero or infinite pitch screws.

Section III-B). Thus, for the purpose of our study, we need to compute the wrench set of any closed-loop mechanism, i.e., mechanisms built as assemblies of multiple serial kinematic chains connected in parallel. If we assume that a closed-loop mechanism is made with m serial kinematic chains connected to a common rigid body (thus creating a closed-loop mechanism), its wrench set $\mathcal{W}$ spans the union of the individual wrench sets of each serial chain [52]

$$\mathcal{W} = \text{span}\left(\mathcal{W}_1 \cup \ldots \cup \mathcal{W}_m\right). \tag{15}$$

For fully constrained mechanisms, the rank of $\mathcal{W}$ is 6, thus, the reciprocal twist set $\mathcal{T}$ is empty, meaning that there is no possible motion of the mechanism, i.e., it is rigid. Singularity analysis deals with finding particular configurations of the closed-loop mechanism where rank $(\mathcal{W}) < 6$, thus leaving the system underconstrained and locally allowing for $6 - \text{rank}\,(\mathcal{W})$ singular twists (reciprocal to $\mathcal{W}$). An example of singularity analysis of an RRR closed-loop mechanism is provided in the Appendix.

In the following section, we recall how a virtual kinematic mechanism can be used to represent the constraints imposed by bearing measurements.

B. Virtual Kinematic Mechanisms

The "hidden robot" is a concept that was initially developed for the analysis of visual servoing singularities [54], and which was recently extended to the mobility and singularity analysis of bearing rigid formations [41]. This concept allows the representation of bearing measurements as a set of kinematic joints linked together by rigid bodies, creating a virtual closed-loop mechanism. The wrench set of this virtual mechanism is shown to be analogous to the constraints imposed by the measurement sets in the fleet of agents. In the general case of a bearing measurement taken in $\mathfrak{F}_i$ and directed to $\mathfrak{F}_j$, the bearing measurement $\boldsymbol{\beta}_{ij}$ geometrically constrains the position of $\mathfrak{F}_j$ expressed in $\mathfrak{F}_i$ (denoted as $\mathbf{p}_{ij}$) to be

$$\mathbf{p}_{ij} = d_{ij}\boldsymbol{\beta}_{ij} \quad \forall d_{ij} > 0. \tag{16}$$

Moreover, a bearing measurement $\boldsymbol{\beta}_{ij}$ does not geometrically constrain the orientation of $\mathfrak{F}_j$ wrt to $\mathfrak{F}_i$. When $\mathfrak{F}_i$ and $\mathfrak{F}_j$ may both move freely in $\text{SE}(3)$, it has been shown in [55] that the geometric constraint introduced by the measurement can be represented as a virtual UPS kinematic chain[2] [see Fig. 3(a)]. The active U joint is centered on $\mathfrak{F}_i$ and controls the direction of the prismatic joint linking $\mathfrak{F}_i$ to $\mathfrak{F}_j$: this direction is given in $\mathfrak{F}_i$ by the bearing $\boldsymbol{\beta}_{ij}$. The combination of the U and P joints constrain $\mathfrak{F}_j$ to move on the line defined by (16). Additionally, the spherical joint is coincident with $\mathfrak{F}_j$, but as it is passive (i.e., its motion is neither controlled nor measured), there is no constraint on the orientation of $\mathfrak{F}_j$ relative to $\mathfrak{F}_i$.

In the case of quadrotors, which have their roll and pitch coupled to translations in the horizontal plane, the virtual mechanism accounts for the underactuation by constraining their roll and pitch to zero [41] (the roll and pitch of the quadrotor is well estimated, thus, any bearing may always be reprojected flat). This reduces the original UPS virtual kinematic chain of a bearing measurement in $\text{SE}(3)$ to a UPRR kinematic chain [see Fig. 3(b)], where the active revolute joint constrains the final passive revolute joint to have a vertical axis, representing the unknown yaw of $\mathcal{A}_j$. A mutual observation between $\mathcal{A}_i$ and $\mathcal{A}_j$ leads to a UPU kinematic chain, constraining the relative yaw between the two agents. Because the singularities in the wrench set of closed-loop mechanisms (i.e., those which correspond to the singularities of the bearing formations) arise due to unconstrained motions of their passive kinematic pairs [56], the active joints may be ignored when representing the virtual mechanisms from here on, leaving only the passive joints. Thus, the UPRR kinematic chain can be simplified to a PR kinematic chain, and the UPU kinematic chain can by simplified to a simple prismatic joint. To facilitate the analysis further on, the screw sets of these virtual mechanisms are fully developed in the following section.

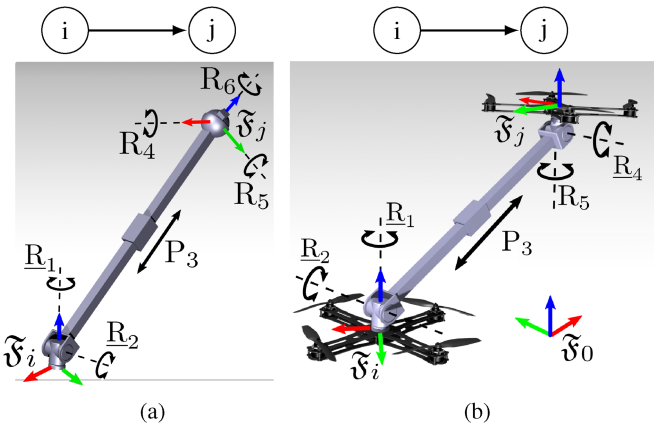

Fig. 3. Virtual mechanism of directed graph edges on $\text{SE}(3)$ (a) and $\mathbb{R}^3 \times \mathcal{S}^1$ (b). (a) Virtual UPS mechanism. (b) Virtual UPRR mechanism.

C. Elementary Twists and Wrenches of the Virtual Kinematic Mechanism of Single Graph Edges

When analyzing formations, we are often required to deal with large sets of screws, which are tedious to represent individually. Furthermore, as it is formations and not the virtual mechanisms that are the subject of the interest, we want to be able to link screw sets to the formation graph. We, therefore, introduce a notation better adapted to large formations, which will be used later in this article. The formation edges will be characterized with respect to $\mathcal{A}_i$ (the other agent being by default $\mathcal{A}_j$), as shown in Fig. 4. The three edge types are as follows.

1) Measurement of $\mathcal{A}_j$ by $\mathcal{A}_i$: This is considered an "out" edge, denoted as $\mathbb{O}$, as the graph edge $\mathcal{E}_{ij}$ leaves the vertex $\mathcal{V}_i$. Following the methodology in [41] and considering only the passive motions (i.e., motions that do not effect the bearing measurements), the virtual mechanism can be simplified to a PR mechanism [see Fig. 4(a)] with the twist set

$$\mathcal{T}_{\mathbb{O}} = \left\{\mathbb{v}^{\text{t}}(\mathbf{p}_{ij}),\ \mathbb{v}^{\text{r}}(\mathbf{z}_0, \mathbf{p}_j)\right\} \tag{17}$$

[2]"U" indicates a universal joint, and "S" a spherical joint, where U and S are, respectively, composed of two and three intersecting orthogonal revolute joints. "P" indicates a prismatic (purely translational) joint. An underline indicates an active (or motorized/measured) joint, otherwise the joint is passive.

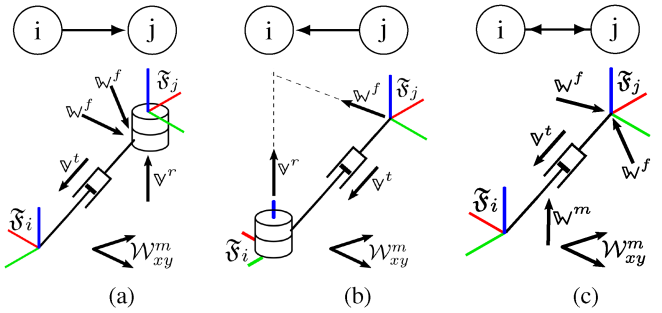

Fig. 4. Out $\mathbb{O}$, in $\mathbb{I}$, and bidirectional $\mathbb{B}$ edges of an agent $\mathcal{A}_i$. These are simply the passive chains of the UPRR (a) and (b) and UPU (c) mechanism in Fig. 3(b). (a) $\mathbb{O}$ edge. (b) $\mathbb{I}$ edge. (c) $\mathbb{B}$ edge.

where $\mathbb{v}^{\mathrm{t}}(\mathbf{p}_{ij})$ is a pure translation twist between $\mathcal{A}_i$ and $\mathcal{A}_j$ directed along β_{ij} in $\mathfrak{F}_i$ ($\mathbf{p}_{ij} = \mathbf{p}_j - \mathbf{p}_i$), and $\mathbb{v}^{\mathrm{r}}(\mathbf{z}_0, \mathbf{p}_j)$ is a pure rotation twist around $\mathbf{z}_0$, with null translational velocity at $\mathbf{p}_j$. Using the reciprocity conditions in Section III-A, the wrench set constraining $\mathcal{A}_j$ to $\mathcal{A}_i$ and expressed at $\mathbf{p}_j$ is, therefore,

$$\mathcal{W}_{\mathbb{O}} = \left\{\mathcal{W}^m_{xy},\ \mathbb{w}^{\mathrm{f}}(\mathbf{p}_{ij}^{\perp 1}, \mathbf{p}_j),\ \mathbb{w}^{\mathrm{f}}(\mathbf{p}_{ij}^{\perp 2}, \mathbf{p}_j)\right\} \tag{18}$$

where $\mathbb{w}^{\mathrm{f}}(\mathbf{p}_{ij}^{\perp k}, \mathbf{p}_j)$ ($k = 1, 2$) are two pure forces orthogonal to the direction $\mathbf{p}_{ij}$ applied at $\mathbf{p}_j$ ($\mathbf{p}_{ij}^{\perp 1}$ and $\mathbf{p}_{ij}^{\perp 2}$ are any two vectors spanning the plane normal to $\mathbf{p}_{ij}$) and they constrain the translational motion of $\mathcal{A}_j$ to lie on the bearing β_{ij}. Moreover, $\mathcal{W}^m_{xy}$ is the set of horizontal moments

$$\mathcal{W}^m_{xy} = \{\mathbb{w}^{\mathrm{m}}(\mathbf{x}_0),\ \mathbb{w}^{\mathrm{m}}(\mathbf{y}_0)\} \tag{19}$$

which constrains the roll and pitch of both quadrotors to zero.

2) Measurement of $\mathcal{A}_i$ by $\mathcal{A}_j$: This is considered an "in" edge, denoted as $\mathbb{I}$, as the graph edge $\mathcal{E}_{ji}$ enters the vertex $\mathcal{V}_i$. The virtual mechanism of this edge has a passive RP structure [see Fig. 3(b)], with the twist set

$$\mathcal{T}_{\mathbb{I}} = \left\{\mathbb{v}^{\mathrm{t}}(\mathbf{p}_{ij}),\ \mathbb{v}^{\mathrm{r}}(\mathbf{z}_0, \mathbf{p}_i)\right\} \tag{20}$$

where $\mathbb{v}^{\mathrm{t}}(\mathbf{p}_{ij})$ is defined below (17) and $\mathbb{v}^{\mathrm{r}}(\mathbf{z}_0, \mathbf{p}_i)$ is a pure rotation twist around $\mathbf{z}_0$, with null translational velocity at $\mathbf{p}_i$. The wrench set constraining $\mathcal{A}_j$ to $\mathcal{A}_i$ expressed at $\mathbf{p}_j$ is

$$\mathcal{W}_{\mathbb{I}} = \left\{\mathcal{W}^m_{xy},\ \mathbb{w}^{\mathrm{f}}(\mathbf{p}_{ij}^{\perp 3}, \mathbf{p}_j),\ \mathbb{w}^{\mathrm{f}}(\mathbf{z}_0 \times \mathbf{p}_{ij}, \mathbf{p}_i)\right\} \tag{21}$$

where $\mathbb{w}^{\mathrm{f}}(\mathbf{p}_{ij}^{\perp 3}, \mathbf{p}_j)$ is the force constraining $\mathcal{A}_j$ to continue observing $\mathcal{A}_i$ along β_{ji}. Its axis $\mathbf{p}_{ij}^{\perp 3}$ is the vector orthogonal to $\mathbf{p}_{ij}$ and intersecting the $\mathbf{z}_0$ axis passing through $\mathfrak{F}_i$. It can be expressed as

$$\mathbf{p}_{ij}^{\perp 3} = [\mathbf{p}_{ij}]_\times [\mathbf{z}_0]_\times \mathbf{p}_{ij}. \tag{22}$$

3) Bidirectional Measurement Between $\mathcal{A}_i$ and $\mathcal{A}_j$: This is considered as a bidirectional edge, denoted as $\mathbb{B}$, because the graph edges $\mathcal{E}_{ij}$ and $\mathcal{E}_{ji}$ can be coalesced into a single edge joining $\mathcal{V}_i$ and $\mathcal{V}_j$, with the intersection of their two twist sets

$$\mathcal{T}_{\mathbb{B}} = \mathcal{T}_{\mathbb{O}} \cap \mathcal{T}_{\mathbb{I}}. \tag{23}$$

Note that due to a limitation of the virtual mechanism analogy, there is a singularity in the leg model when $\mathbf{p}_{ij}$ is vertical: in this case, the rotation of the agent $\mathcal{A}_j$ with respect to the agent $\mathcal{A}_i$ cannot be constrained anymore, leading to the removal of $\mathbb{w}^{\mathrm{m}}(\mathbf{z}_0)$ from $\mathcal{W}_{\mathbb{B}}$, effectively turning the $\mathbb{B}$ edge into an $\mathbb{O}$ edge. In this case, as both agents necessarily lie on the screw axis of the R joint, the exact placement of the R joint between $\mathcal{A}_i$ and $\mathcal{A}_j$ is irrelevant. The twist set $\mathcal{T}_{\mathbb{B}}$ is, therefore

$$\mathcal{T}_{\mathbb{B}} = \begin{cases} \{\mathbb{v}^{\mathrm{t}}(\mathbf{p}_{ij}),\ \mathbb{v}^{\mathrm{r}}(\mathbf{z}_0, \mathbf{p}_j)\} & \text{if } \mathbf{p}_{ij} \propto \mathbf{z}_0 \\ \{\mathbb{v}^{\mathrm{t}}(\mathbf{p}_{ij})\} & \text{otherwise} \end{cases} \tag{24}$$

and the reciprocal wrenches constraining $\mathcal{A}_j$ relative to $\mathcal{A}_i$ expressed at $\mathbf{p}_j$ are, thus

$$\mathcal{W}_{\mathbb{B}} = \begin{cases} \{\mathcal{W}_{\mathbb{O}}\} & \text{if } \mathbf{p}_{ij} \propto \mathbf{z}_0 \\ \{\mathcal{W}_{\mathbb{O}},\ \mathbb{w}^{\mathrm{m}}(\mathbf{z}_O)\} & \text{otherwise} \end{cases} \tag{25}$$

which is similar to $\mathcal{W}_{\mathbb{O}}$, but with an additional constraint on the relative yaw so long as the $\mathbb{B}$ is not singular. It is important to remark that in all cases $\mathcal{W}_{\mathbb{O}}$ and $\mathcal{W}_{\mathbb{I}}$ are both subsets of $\mathcal{W}_{\mathbb{B}}$

$$\mathcal{W}_{\mathbb{O}} \subset \mathcal{W}_{\mathbb{B}} \tag{26a}$$

$$\mathcal{W}_{\mathbb{I}} \subset \mathcal{W}_{\mathbb{B}}. \tag{26b}$$

Another noteworthy remark is that the twist set of each edge type contains at least one twist, thus, every agent must have graph edges connecting it to at least two distinct agents in order to fully constrain it to the rest of the formation.

This section showed how the bearing formation may be represented as a virtual kinematic mechanism, which is the first step in the geometric analysis of singularities. Then, by using the conditions of reciprocity of screws provided in Section III-A, it is possible to identify the singularities of the wrench set, and thus, of the bearing rigidity matrix as in done in [41]. For the following section, we show how we propose extending this study of singularities to large formations, which until now have been too complicated to analyze.

IV. Methodology for Formation Singularity Analysis

There have been decades of extensive work in the robotics community dedicated to the singularity analysis of serial and parallel kinematic chains. However, these works cannot be directly applied to multiagent formations in a general manner because classical parallel mechanisms have a relatively limited number of bodies, while today decentralized UAV formations may have tens, and in the future possibly hundreds or thousands of agents [57]. Consider an arbitrary generically rigid formation with n agents and m edges. Fixing agent $\mathcal{A}_1$ in position and yaw restricts the formation such that the only nonsingular motion of each agent $\mathcal{A}_i\ \forall i \in [2, n]$ is a uniform expansion of the formation about $\mathcal{A}_1$. Each agent, therefore, has a single twist, and thus, five wrenches. As each directed edge exerts four wrenches, we have a system of 4 m wrenches with a rank of $5(n-1)$. As singularity analysis for parallel robots with a single 6 DOF rigid platform constrained by six wrenches is often a challenging task, finding conditions for which the rank of this system with $(n-1)$ DOF constrained by 4 m wrenches degenerates becomes impractically difficult as m and n become large. Furthermore, classical singularity analysis focuses on finding singularities in a single mechanism, or a limited class of mechanisms. For

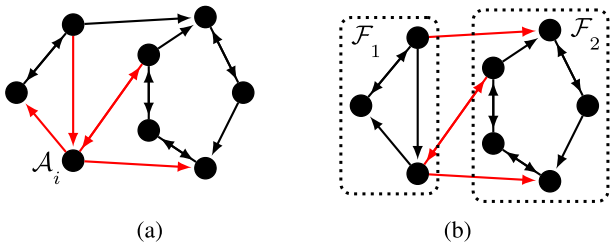

Fig. 5. Singularity analysis methods using local and subformation subsystems of a graph, with the analyzed edges drawn in red. (a) Local analysis. (b) Subformation analysis.

formations, the topology of which may change as graph edges are formed and broken in real time, there are simply too many combinations to individually solve all their singularities. The problem becomes then combinatorial and cannot be handled by hand.

Due to the fact that there is currently no universal method of analyzing the singularities of large multiloop mechanisms, we are unable to propose a general methodology for the complete characterization of all singularities of all formations. Instead, what we propose in this article is a method of classifying the singularities of rigid formations, such that many formations may be completely analyzed based on their graph structure. By decomposing the graph into subgraphs (as shown in Fig. 5), we are able to analyze the singularities of many very large graphs. Furthermore, in Section VII, we show that we can design formation graphs with an almost infinite number of agents for which the singularities are completely known. To achieve this we consider the following two simple principles.

1) If any agent moves with respect to the rest of the formation which is fixed, the formation is singular.
2) If any group of agents moves with respect to the rest of the formation which is fixed, the formation is singular.

Based on these principles, it is worth mentioning that local singularities are a subset of subformation singularities where one of the two subformations is restricted to a single agent. However, as it will be shown later, the analysis of the singularities of the subformation with more than a single agent is much more complex than the analysis of the local singularities, which is the reason why we prefer to decouple these two analyses in this way in what follows.

These two principles lead to the decomposition of the study of formation singularities into local (denoted by $\mathcal{S}^L$) and subformation (denoted by $\mathcal{S}^F$) singularities. These are used to study the formation graph decomposed into subgraphs as shown in Fig. 5 and attempt to answer the questions. Let us start by defining subformation singularity.

a) Subformation singularity: Can a group of agents move with respect to another group of agents, assuming both groups are rigid? Mathematically speaking, subformation singularities can be defined as follows. Here, we provide the mathematical definition for two subformations, but the definition can be extended to more complex cases.

Let us consider a formation $\mathcal{F}(\mathcal{G},\ \mathbf{q})$, which is generically rigid, i.e., for which $\text{rank}\,(\mathcal{N}_{\mathbf{B}(\mathbf{q})}) = \text{rank}\,(\mathbf{V}_{\mathfrak{M}})$, for an arbitrary formation embedding $\mathbf{q}$. This formation can be partitioned into two subformations $\mathcal{F}_A(\mathcal{G}_A,\ \mathbf{q}_A)$ and $\mathcal{F}_B(\mathcal{G}_B,\ \mathbf{q}_B)$ connected together by a set of bearings $\boldsymbol{\beta}_{AB}$. $\mathcal{F}_A(\mathcal{G}_A,\ \mathbf{q}_A)$ and $\mathcal{F}_B(\mathcal{G}_B,\ \mathbf{q}_B)$ are also considered to be generically rigid, i.e., $\text{rank}\,(\mathcal{N}_{\mathbf{B}_A(\mathbf{q}_A)}) = \text{rank}\,(\mathbf{V}_{\mathfrak{M}_A})$, $\text{rank}\,(\mathcal{N}_{\mathbf{B}_B(\mathbf{q}_B)}) = \text{rank}\,(\mathbf{V}_{\mathfrak{M}_B})$, where $\mathbf{B}_A$ ($\mathbf{B}_B$, resp.) is the rigidity matrix of the subformation $\mathcal{F}_A$ ($\mathcal{F}_B$, resp.), and $\mathfrak{M}_A$ ($\mathfrak{M}_B$, resp.) is the set of its trivial motions.

For a formation velocity vector $\dot{\mathbf{q}} \notin \mathbf{V}_{\mathfrak{M}}$ defined such that $\dot{\mathbf{q}} = [\dot{\mathbf{q}}_A^T\ \dot{\mathbf{q}}_B^T]^T$, with $\dot{\mathbf{q}}_A = \mathbf{0}$ and $\dot{\mathbf{q}}_B \neq \mathbf{0}$ (or $\dot{\mathbf{q}}_A \neq \mathbf{0}$ and $\dot{\mathbf{q}}_B = \mathbf{0}$), if it exists a configuration $\mathbf{q}^*$ such that $\mathbf{B}(\mathbf{q}^*)\dot{\mathbf{q}} = \mathbf{0}$, the formation $\mathcal{F}$ is in subformation singularity at $\mathbf{q}^*$. This condition implies that there exists a relative motion between the subformations $\mathcal{F}_A$ and $\mathcal{F}_B$ out of the permitted motions $\mathbf{V}_{\mathfrak{M}}$: Again, the graph is not rigid anymore. This relative motion can be infinitesimal (in most of cases) or finite (for instance, if all bearings are parallel to each others).

b) Local singularity: Can an individual agent move with respect to its neighbors, assuming that the neighbors are rigid? As mentioned earlier, local singularities are a subset of subformation singularities with two partitions $\mathcal{F}_A(\mathcal{G}_A,\ \mathbf{q}_A)$ and $\mathcal{F}_B(\mathcal{G}_B,\ \mathbf{q}_B)$, one of them being restricted to a single point.

This type of analysis is limited in that we cannot prove that all singularities in all possible rigid graphs are detected. Indeed, there are limitations in the scope of the subformation analysis (see Section VI-D). We are, however, still able to find many singularities in those graphs for which we cannot guarentee that all singularities are identified. We do show, however, in Section VII that arbitrarily large formations can be built for which the singularities are fully identified (i.e., all singular embeddings of the formation are spanned by a known set of $\mathcal{S}^L \cup \mathcal{S}^F$).

In Sections V–VI, we provide details on the local and subformation singularities types. Only the methodology and main results are hereafter.

V. Characterization of Local Singularities

We recall that the analysis of the local singularities $\mathcal{S}_i^L$ of $\mathcal{A}_i$ assumes that all other agents are rigid. It then follows that any change in interagent distance between any two agents other than $\mathcal{A}_i$ is necessarily contained in $\mathfrak{M}$, and more precisely, in the uniform expansion of the formation. As there is necessarily at least two distinct graph edges in any local formation, we may fix the distance between all agents other than $\mathcal{A}_i$, permitting a direct application of the analysis method used for classical parallel kinematic mechanisms. Applying the method described in Section III-B to recover the hidden robot and fixing the interagent distance of the agents other than $\mathcal{A}_i$, the local wrench set $\mathcal{W}_i$ constraining $\mathcal{A}_i$ to the rest of the formation may be found as the union of the wrench sets of the local edges constraining $\mathcal{A}_i$ to its neighbors. This may be expressed as

$$\mathcal{W}_i = \bigcup_{\forall \mathcal{E}_{ij}, \mathcal{E}_{ji} \in \mathcal{E}} \mathcal{W}_j \tag{27}$$

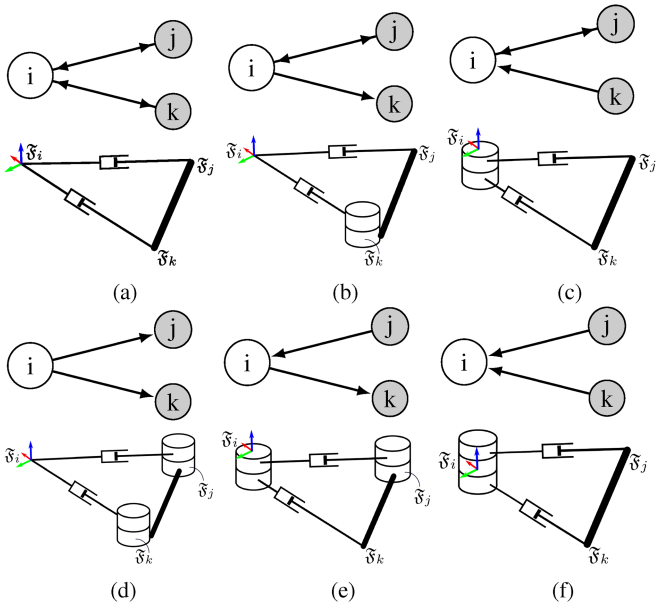

Fig. 6. All unique local formations of $\mathcal{A}_i$ connected with two other agents (shaded). The thick lines represent rigid links. (a) $L_{\mathbb{BB}}$. (b) $L_{\mathbb{BO}}$. (c) $L_{\mathbb{BI}}$. (d) $L_{\mathbb{OO}}$. (e) $L_{\mathbb{IO}}$. (f) $L_{\mathbb{II}}$.

where $\mathcal{W}_j$ is the set of wrenches constraining $\mathcal{A}_j$ to $\mathcal{A}_i$. In the following sections, we present all possible singularities for local formations with an arbitrary number of edges.

A. Local Singularities With Two Edges

In Fig. 6, all six possible nonisomorphic local formations composed of two distinct edges joining $\mathcal{A}_i$ to $\mathcal{A}_j$ and $\mathcal{A}_k$ are shown, along with their corresponding virtual mechanisms. As there are few combinations, these may all be subjected to a singularity analysis using screw theory, as presented in Section III-A. The set of local singular configurations of $\mathcal{A}_i$, denoted by $\mathcal{S}_i^L$, contains all embeddings of L_i where the wrench set $\mathcal{W}_i$ degenerates to rank $(\mathcal{W}_i) < 6$. We exploit the fact that $\mathcal{W}_{\mathbb{O}} \subset \mathcal{W}_{\mathbb{B}}$ and $\mathcal{W}_{\mathbb{I}} \subset \mathcal{W}_{\mathbb{B}}$, remarking that if $\mathcal{W}_i$ is degenerate in a configuration, any subset of $\mathcal{W}_i$ must also be degenerate in that configuration. As such, it makes sense to begin with the local formation $L_{\mathbb{BB}}$ where $\mathcal{A}_i$ has two bidirectional $\mathbb{B}$ edges.

The wrench set $\mathcal{W}_{\mathbb{BB}}$ in a generic configuration is spanned by the system

$$\mathcal{W}_{\mathbb{BB}}^L = \begin{cases} \mathcal{W}_{xy}^m, \ \mathbb{w}^{\mathrm{m}}(\mathbf{z}_0) \\ \mathbb{w}_{j1}^{\mathrm{f}}(\mathbf{p}_{ij}^{\perp 1}, \mathbf{p}_j), \ \mathbb{w}_{j2}^{\mathrm{f}}(\mathbf{p}_{ij}^{\perp 2}, \mathbf{p}_j) \\ \mathbb{w}_{k1}^{\mathrm{f}}(\mathbf{p}_{ik}^{\perp 1}, \mathbf{p}_k), \ \mathbb{w}_{k2}^{\mathrm{f}}(\mathbf{p}_{ik}^{\perp 2}, \mathbf{p}_k). \end{cases} \tag{28}$$

Using the methodology outlined in Section III-A, it can be found that there are two geometric conditions resulting in singularities

$$\mathcal{S}_{\mathbb{BB}}^L = \begin{cases} 1. \ \mathbf{p}_{ij} \text{ and } \mathbf{p}_{ik} \text{ are colinear} \\ 2. \ \mathbf{p}_{ij} \text{ and } \mathbf{p}_{ik} \text{ are vertical} \end{cases}$$

with the second condition being a subset of the first and allowing an additional singular twist.

TABLE I
SINGULARITIES FOR 2-EDGE LOCAL FORMATIONS OF $\mathcal{A}_i$ CONNECTED TO AGENTS $\mathcal{A}_j$ AND $\mathcal{A}_k$ (SEE FIG. 6)

Type	Wrenches	Singular configuration $\mathcal{S}_{\text{type}}^L$
$L_{\mathbb{BB}}$	$\mathcal{W}_{\mathbb{B}j} \cup \mathcal{W}_{\mathbb{B}k}$	1. $\mathcal{S}_{\mathbb{BB}}^L$
$L_{\mathbb{BO}}$	$\mathcal{W}_{\mathbb{B}j} \cup \mathcal{W}_{\mathbb{O}k}$	1. $\mathcal{S}_{\mathbb{BB}}^L$
$L_{\mathbb{BI}}$	$\mathcal{W}_{\mathbb{B}j} \cup \mathcal{W}_{\mathbb{I}k}$	1. $\mathcal{S}_{\mathbb{BB}}^L$ 2. $\mathbf{p}_{ij}$ is vertical
$L_{\mathbb{OI}}$	$\mathcal{W}_{\mathbb{O}j} \cup \mathcal{W}_{\mathbb{I}k}$	1. $\mathcal{S}_{\mathbb{BI}}^L$ 2. $\mathbf{p}_{ij} \times \mathbf{p}_{ik}$ is vertical
$L_{\mathbb{OO}}$	$\mathcal{W}_{\mathbb{O}j} \cup \mathcal{W}_{\mathbb{O}k}$	1. $\mathcal{S}_{\mathbb{OI}}^L$ 2. $\mathbf{p}_{jk}$ is vertical
$L_{\mathbb{II}}$	$\mathcal{W}_{\mathbb{I}j} \cup \mathcal{W}_{\mathbb{I}k}$	1. $\mathcal{S}_{\mathbb{BI}}^L$ 2. All configurations

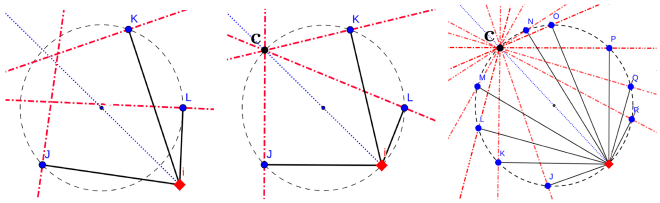

Fig. 7. Singularity analysis of the $\mathbb{OOO}$ (a) and (b) and $\mathbb{O}^{\mathrm{n}}$ (c) type local subformations on the horizontal plane. The red square is $\mathcal{A}_i$, the blue circles denote agents $\mathcal{A}_a \forall a$, and the red lines represent the force component of $\mathcal{W}_{\mathbb{O}}$ that lies in the horizontal plane. The other force components of the $\mathcal{W}_{\mathbb{O}}$ are orthogonal to the plane and pass through each blue dot. (a) Nonsingular planar configuration. (b) Singular planar configuration. (c) Singular planar configuration.

As all other two-edge local formation wrench sets are a subset of $\mathcal{W}_{\mathbb{BB}}$, the set of singular configurations $\mathcal{S}_{\mathbb{BB}}^L$ is contained within all the other two-edge local singularity sets. An analysis of the hidden robots allows us give all local singularities for a subformation with two edges, and results are summarized in Table I.

B. Local Singularities With Three Edges

We can perform the same analysis for the 10 possible nonisomorphic local formations of $\mathcal{A}_i$ having three neighbors ($\mathcal{A}_j$, $\mathcal{A}_k$, $\mathcal{A}_l$). This is simplified by the knowledge that for any 3-edge wrench set to degenerate, each of the three 2-edge wrench subsets of the 3-edge wrench set must also be degerate. Thus, for our local formation $L_{\mathbb{BBB}}$ with three bidirected edges to become singular, it is necessary that each pair of edges also be singular. This results in the set of singular conditions

$$\mathcal{S}_{\mathbb{BBB}}^L = \begin{cases} 1. \ \mathbf{p}_{ij}, \mathbf{p}_{ik}, \text{ and } \mathbf{p}_{il} \text{ are colinear} \\ 2. \ \mathbf{p}_{ij}, \mathbf{p}_{ik}, \text{ and } \mathbf{p}_{il} \text{ are vertical.} \end{cases}$$

Table II presents the list of singularities for all 3-edge local formations. Additionally, Fig. 7 shows the case when all agents are on a horizontal plane, and the horizontal force component of each wrench set $\mathcal{W}_{\mathbb{O}}$ is drawn in red. In such special case, there is an unconstrained rotation about the point of intersection of

TABLE II
SINGULARITIES FOR 3-EDGE LOCAL FORMATIONS OF $\mathcal{A}_i$ CONNECTED TO AGENTS $\mathcal{A}_j$, $\mathcal{A}_k$, AND $\mathcal{A}_l$

Type	Singular configuration $\mathcal{S}^L_{\text{type}}$
$L_{\mathbb{BBB}}$	$\mathcal{S}^L_{\mathbb{BBB}}$
$L_{\mathbb{BBO}}$	$\mathcal{S}^L_{\mathbb{BBB}}$
$L_{\mathbb{BBI}}$	1. $\mathcal{S}^L_{\mathbb{BBB}}$ 2. $\mathbf{p}_{ij}$ and $\mathbf{p}_{ik}$ are vertical
$L_{\mathbb{BOO}}$	$\mathcal{S}^L_{\mathbb{BBB}}$
$L_{\mathbb{BOI}}$	$\mathcal{S}^L_{\mathbb{BBI}}$
$L_{\mathbb{BII}}$	1. $\mathcal{S}^L_{\mathbb{BBI}}$ 2. $\mathbf{p}_{ij}$ is vertical
$L_{\mathbb{OOO}}$	1. $\mathcal{S}^L_{\mathbb{BBB}}$ 2. $\mathcal{A}_{i,j,k,l}$ lie on a common circle in a horizontal plane 3. $\mathcal{A}_{j,k,l}$ are vertical
$L_{\mathbb{OOI}}$	$\mathcal{S}^L_{\mathbb{BBI}}$
$L_{\mathbb{OII}}$	$\mathcal{S}^L_{\mathbb{BII}}$
$L_{\mathbb{III}}$	1. $\mathcal{S}^L_{\mathbb{BBB}}$ 2. All configurations

the forces, which is diametrically opposite to $\mathcal{A}_i$ on the circle, and corresponds to the center of rotation $\mathbf{c}$.

C. Local Singularities With Many Edges

Assuming $\mathcal{A}_i$ is connected to m other agents and each graph edge $\mathcal{E}_{ia} \forall a \in [1, m]$ is associated with a wrench set $\mathcal{W}_a$, the local wrench set $\mathcal{W}_i$ constraining $\mathcal{A}_i$ to the rest of the formation is given by (15). Continuing to add edges connecting $\mathcal{A}_i$ to more and more agents, we further constrain the system. Any degeneracy of the augmented constraint system must then lie within the singularity space of the original system as well as that of the new constraints. The singularity set $\mathcal{S}^L_i$ of the local formation of $\mathcal{A}_i$ containing m agents then becomes the intersection of all possible combinations of the two edge singularity sets

$$\mathcal{S}^L_i = \mathcal{S}^L_{12} \cap \mathcal{S}^L_{13} \cap \ldots \cap \mathcal{S}^L_{1\,m} \cap \ldots \cap \mathcal{S}^L_{(m-1)m} \tag{29}$$

which is a compact (and quite small for large m values) set.

For agents with many edges, it is simple to extrapolate any local formation from the results of Table II by applying the following rules to any local formation of type $L_{\mathbb{B}^a\mathbb{O}^b\mathbb{I}^c}$ with a $\mathbb{B}$ edges, b $\mathbb{O}$ edges, and c $\mathbb{I}$ edges ($m = a + b + c \geq 3$).

1) Singularities of all local formations of type $L_{\mathbb{B}^a\mathbb{O}^b\mathbb{I}^c}$.
   a) All edges are colinear.
   b) All $\mathbb{B}$ edges and all $\mathbb{O}$ edges are vertical (note that this corresponds to type $L_{\mathbb{I}^c}$ for all embeddings).
2) Singularities of local formations of type $L_{\mathbb{O}^m}$.
   a) Agents $\mathcal{A}_i$ and $\mathcal{A}_1 \cdots \mathcal{A}_m$ lie on a common horizontal circle [see Fig. 7(c)].
   b) Agents $\mathcal{A}_1 \cdots \mathcal{A}_m$ share a common vertical axis.

All local singularities are sufficient conditions for the formation to lose rigidity. However, as the analysis is predicated on a potentially flawed hypothesis (that all agents in L_i other than $\mathcal{A}_i$ are rigid), the lack of local singularities is only a necessary condition to demonstrate rigidity. As such, in the following section, we extend the analysis to distinct groups of agents within a given formation, i.e., the analysis of subformation singularities.

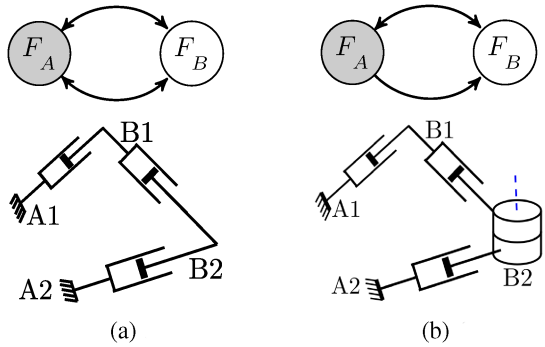

Fig. 8. Two subsystems $\mathcal{F}_A$ and $\mathcal{F}_B$ connected by two distinct graph edges. Agents $A_i \in \mathcal{F}_A$, agents $B_i \in \mathcal{F}_B$. Bearings $\boldsymbol{\beta}_{ij}$ are along lines A_iB_i. (a) $\mathcal{F}_{\mathbb{BB}}$. (b) $\mathcal{F}_{\mathbb{BO}}$.

VI. CHARACTERIZATION OF SUBFORMATION SINGULARITIES

Subformation singularities [see Fig. 5(b)] analyze the interaction between two presumably rigid subformations $\mathcal{F}_A$ and $\mathcal{F}_B$ of the formation $\mathcal{F}_{AB}$. This analysis is in fact a superset of the local singularity analysis, which arise when $\mathcal{F}_A$ or $\mathcal{F}_B$ contains only a single agent. As such, here we only consider the untreated case of both subformations containing more than one agent.

To analyze these singularities, we fix the agents of $\mathcal{F}_A$ in place and assume that $\mathcal{F}_A$ and $\mathcal{F}_B$ are intrinsically rigid. This will fully constraint the trivial motions of $\mathcal{F}_{AB}$, and the fixed agents of $\mathcal{F}_A$ become the "ground link" of a classical parallel kinematic chain. The unfixed subformation $\mathcal{F}_B$ may then modeled only by those of its agents interacting with $\mathcal{F}_A$. These agents are constrained in space by the edges connecting the two subformations, but are also subject to constraints within their own subformation, thus are modeled as being connected by prismatic joints allowing only a scaling of $\mathcal{F}_B$. As the trivial motions of $\mathcal{F}_{AB}$ are fixed by $\mathcal{F}_A$, any mobility of any agent in $\mathcal{F}_B$ is necessarily singular.

A. Subformation Singularities With Two Edges

Considering the case where $\mathcal{F}_A$ and $\mathcal{F}_B$ are connected by two edges, as shown in Fig. 8, there are only two possible rigid two-edge subformation types: $F_{\mathbb{BB}}$ and $F_{\mathbb{BO}}$, where the two subformations are connected by either two bidirectional edges, or by a bidirectional edge and a directed edge. The subformation type $F_{\mathbb{BI}}$ is the same as $F_{\mathbb{BO}}$, just viewed from the perspective of F_B instead of F_A, and the other possible types ($F_{\mathbb{OO}}$ and $F_{\mathbb{OI}}$) are not generically rigid.

Starting with an analysis $F_{\mathbb{BB}}$ because its singularities are necessarily also those of $F_{\mathbb{BO}}$, the wrench set constraining $\mathcal{F}_A$ to $\mathcal{F}_B$ is

$$\mathcal{W}^F_{\mathbb{BB}} = \begin{cases} \mathcal{W}^m_{xy},\ \mathbb{w}^{\mathrm{m}}(\mathbf{z}_0) \\ \mathbb{w}^{\mathrm{f}}_{11}(\mathbf{p}_{A1B1} \times \mathbf{p}_{B1B2}, \mathbf{p}_{B2}) \\ \mathbb{w}^{\mathrm{f}}_{21}(\mathbf{p}^{\perp 1}_{A2B2}, \mathbf{p}_{B2}),\ \mathbb{w}^{\mathrm{f}}_{22}(\mathbf{p}^{\perp 2}_{A2B2}, \mathbf{p}_{B2}). \end{cases} \tag{30}$$

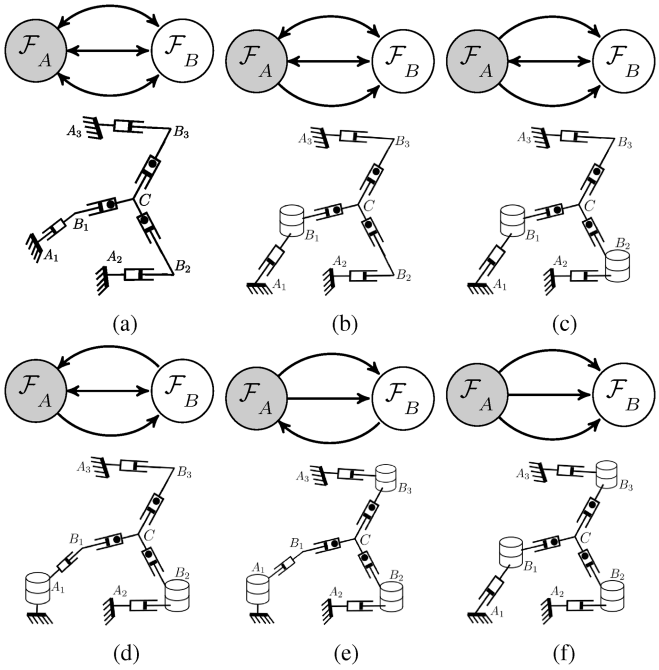

Fig. 9. All combinations of two subsystems $\mathcal{F}_A$ and $\mathcal{F}_B$ connected by three distinct directed graph edges. All prismatic joints containing a circle have coupled twist magnitudes. Note that the center of expansion C of subformation $\mathcal{F}_B$ can be placed at any finite point in $\mathbb{R}^3$. Agents $A_i \in \mathcal{F}_A$, agents $B_i \in \mathcal{F}_B$. Bearings $\boldsymbol{\beta}_{ij}$ are along lines A_iB_i. (a) $F_{\mathbb{BBB}}$. (b) $F_{\mathbb{OBB}}$. (c) $F_{\mathbb{OOB}}$. (d) $F_{\mathbb{IOB}}$. (e) $F_{\mathbb{IOO}}$. (f) $F_{\mathbb{OOO}}$.

This wrench set degenerates under the singular conditions $\mathcal{S}^F_{\mathbb{BB}}$.

1) *The two lines A_1B_1 and A_2B_2 intersect:* The wrench $\mathbb{w}^{\mathrm{f}}_{11}$ falls within the span of $\mathbb{w}^{\mathrm{f}}_{21}$ and $\mathbb{w}^{\mathrm{f}}_{22}$, thus rank $(\mathcal{W}^F_{\mathbb{BB}}) = 5$. The singular twist is an expansion of F_B about the point of intersection P.
2) *The two lines are colinear:* This is a special case of 1), resulting in F_B having an unconstrained twist $\mathbb{v}^{\mathrm{t}}(A_1B_1)$ with respect to F_A, as well as an expansion about any point lying on the colinear lines.
3) *The two lines are colinear and vertical:* This case is a special case of 2), introducing an unconstrained rotational twist $\mathbb{v}^{\mathrm{r}}(\mathbf{z}_0, A_1)$ between the two suformations.

The formation type $F_{\mathbb{BO}}$ degenerates under the same conditions as $F_{\mathbb{BB}}$, with an additional singularity occurring when the $\mathbb{B}$ is vertical, reducing the wrench set to that of a $F_{\mathbb{OO}}$ subformation, which in nonrigid.

B. Subformation Singularities With Three Edges

There are six possible architectures of two subformations joined by three edges, all of which are shown in Fig. 9, and all of which are generically rigid. With these formations, we must adapt the virtual mechanism structure to account for F_Bs ability to expand about a finite point C. To this end, we define a coupled prismatic joint, where the twist velocity is necessarily proportional to the length of the joint.

Four of the six architectures (all those which contain a $\mathbb{B}$ edge) have singularity sets, which are necessarily subsets of the known two-edge rigid subformations' sets of singularities,

TABLE III
CLASSIFICATION OF ALL BIPARTITIONED SUBFORMATION SINGULARITIES WITH TWO OR THREE EDGES

Type	Singular Configuration $\mathcal{S}^F_{type}$
$\mathbb{BB}$	1: Lines A_1B_1 and A_2B_2 intersect 2: Lines A_1B_1 and A_2B_2 are parallel
$\mathbb{BO}$	1: $\mathcal{S}^F_{\mathbb{BB}}$ 2: Line A_1B_1 is vertical and intersects B_2
$\mathbb{BBB}$	1: All lines A_iB_i intersect 2: All lines A_iB_i are parallel
$\mathbb{OBB}$	1: $\mathcal{S}^F_{\mathbb{BBB}}$ 2: $A_iB_i, i \in 2, 3$ vertical and superposed, with B_1 on the line A_2B_2
$\mathbb{OOB}$	1: $\mathcal{S}^F_{\mathbb{OBB}}$ 2: A_3B_3 vertical & B_1, B_2 on the line A_3B_3
$\mathbb{IOB}$	1: $\mathcal{S}^F_{\mathbb{OBB}}$ 2: A_3B_3 vertical & A_1, B_2 on the line A_3B_3
$\mathbb{IOO}$	1: $\mathcal{S}^F_{\mathbb{IOB}}$ 2: A_1 and B_2 or B_3 on the same vertical line 3: All agents A_i, B_i $\forall i$ lie on a common horizontal plane 4: Lines A_2B_2 and A_3B_3 are horizontal and the intersection of two horizontal lines passing through the projections of B_2 and B_3 in an horizontal plane is on the vertical axis passing through A_1.
$\mathbb{OOO}$	1: $\mathcal{S}^F_{\mathbb{OOB}}$ 2: B_1, B_2, B_3 aligned and vertical 3: All agents A_i, B_i $\forall i$ lie on a common horizontal plane 4: lines A_jB_j and A_kB_k are horizontal (for $j, k = 1, 2$ or 3, $j \neq k$) and the intersection of two horizontal lines passing through the projections of B_j and B_k in an horizontal plane is on the vertical axis passing through B_i (for $i = 1, 2$ or 3, $i \neq j, k$). 5: $\mathcal{F}_A$ and $\mathcal{F}_B$ are bearing-congruent.

as they contain the two-edge wrench sets along with additional constraints. We can, therefore, determine that

$$\mathcal{S}^F_{\mathbb{BBB}} = \mathcal{S}^F_{\mathbb{BB}} \cap \mathcal{S}^F_{\mathbb{BB}} \cap \mathcal{S}^F_{\mathbb{BB}} \tag{31a}$$

$$\mathcal{S}_{\mathbb{OBB}} = \mathcal{S}^F_{\mathbb{OB}} \cap \mathcal{S}^F_{\mathbb{OB}} \cap \mathcal{S}^F_{\mathbb{BB}} \tag{31b}$$

$$\mathcal{S}_{\mathbb{OOB}} = \mathcal{S}^F_{\mathbb{OO}} \cap \mathcal{S}^F_{\mathbb{OB}} \cap \mathcal{S}^F_{\mathbb{OB}} \tag{31c}$$

$$\mathcal{S}_{\mathbb{IOB}} = \mathcal{S}^F_{\mathbb{IO}} \cap \mathcal{S}^F_{\mathbb{IB}} \cap \mathcal{S}^F_{\mathbb{OB}} \tag{31d}$$

for which we may find definite sets of geometric conditions for singularities (see Table III).

More challenging to analyze are the two types without rigid subtypes, $F_{\mathbb{IOO}}$ and $F_{\mathbb{OOO}}$. Results are found based on screw theory analysis and they are summarized as follows.

1) All agents in $\mathcal{F}_A$ and $\mathcal{F}_B$ are coplanar for $F_{\mathbb{IOO}}$ and $F_{\mathbb{OOO}}$.
2) *$\mathcal{F}_A$ and $\mathcal{F}_B$ are Congruent for $F_{\mathbb{OOO}}$:* Any rigid formation $\mathcal{F}(\mathcal{G}, \mathbf{q})$ defined by a set of bearings $\boldsymbol{\beta}(\mathbf{q})$ may be transformed by an arbitrary differentiable trivial motion $\mathfrak{M}$ to a planar congruent formation $\mathcal{F}(\mathcal{G}, \mathbf{q}^*)$ such that $\boldsymbol{\beta}(\mathbf{q}) = \boldsymbol{\beta}(\mathbf{q}^*)$ [see Fig. 10(c)].

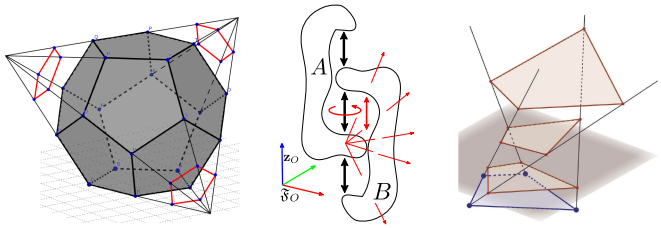

Fig. 10. Examples of singular motions (in red) between subformations in constraint singular embeddings. (a) 20-agent formation is arranged such that each agent lies on the vertex of a regular dodecahedron, and observes each of the three adjacent agents. (b) General bipartitioned formation displaying three singular DOF. (c) Singular motion between F_A (blue) and F_B (red), when all observations are unidirectional from F_A to F_B (i.e., of type $\mathcal{S}^F_{\mathbb{O}^4}$), and the set of observed and observing agents are congruent. (a) Type $\mathbb{B}^5$. (b) Any type. (c) Type $\mathbb{O}^n$.

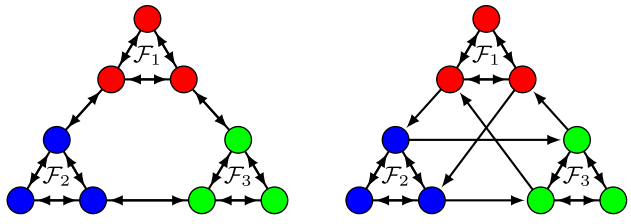

Fig. 11. Two intuitively tri-partionable graphs, composed of three distinct rigid subformations interacting with each other. (a) Generically flexible graph. (b) Generically rigid graph.

3) *For the Formation $F_{\mathbb{OOO}}$:* Lines A_jB_j and A_kB_k are horizontal (for $j,k=1,2,$ or $3, j\neq k$) and the intersection of two horizontal lines passing through the projections of B_j and B_k in an horizontal plane is on the vertical axis passing through B_i (for $i=1,2,$ or $3, i\neq j,k$).
4) *For the Formation $F_{\mathbb{IOO}}$:* Lines A_2B_2 and A_3B_3 are horizontal and the intersection point of two horizontal lines passing through the projections of B_2 and B_3 in an horizontal plane is on the vertical axis passing through A_1.

C. Subformation Singularities With Many Edges

As additional edges between two subformations only adds constraints between them, we can determine (as shown in Section V-C) that there is a compact set of singular conditions for all possible edge combinations. Considering subformations $\mathcal{F}_A$ and $\mathcal{F}_B$, which are joined by a $\mathbb{B}$ edges, b $\mathbb{O}$ edges, and c $\mathbb{I}$ edges, where $m=a+b+c>3$. The singular conditions $\mathcal{S}^F_{\mathbb{B}^a\mathbb{O}^b\mathbb{I}^c}$ are [see Fig. 10].

1) All edges intersect at a common point P.
   a) Generally, $\mathcal{F}_B$ expands with respect to $\mathcal{F}_A$ about point C.
   b) When all edges are colinear, $\mathcal{F}_B$ translates with respect to $\mathcal{F}_A$ and independently expands about any finite point on the line.
   c) When all bearings are vertical and colinear, the previous singular motion is augmented by an additional singular rotation about the colinear bearing.
2) All $\mathbb{B}$ edges are vertical and colinear, intersecting all agents in $\mathcal{F}_B$, which are part of an $\mathbb{O}$ edge, and intersecting all agents in $\mathcal{F}_A$, which are part of an $\mathbb{I}$ edge.

There is an additional singularity $\mathcal{S}^F_{\mathbb{O}^n}$ (and therefore of $\mathcal{S}^F_{\mathbb{I}^n}$ as well) for formations where all edges are directed from one subformation to another. Of course, $\mathcal{S}^F_{\mathbb{O}^n}$ contains the previously listed singular conditions, but it is also singular whenever $\mathcal{F}_A$ and $\mathcal{F}_B$ are bearing-congruent, as is the case in Fig. 10(c). This allows for a 1 DOF coupled translation, rotation, and expansion of $\mathcal{F}_B$ relative to $\mathcal{F}_A$.

D. Subformations Requiring Higher Level Partitioning

For some formations, such as those shown in Fig. 11, it may be necessary to explore higher level partitioning methods, which would be analogous to the singularities of multiplatform parallel robots. In each of the figures shown, an intuitive choice of subformations (or indeed mathematically by spectral clustering [34], [37]) will lead to the analysis of the three rigid subformations F_1, F_2, and F_3. The methodology hitherto presented would call for an analysis of the constraints between F_1 and $F_2\cup F_3$ (and the other two combinations), which would have singularities of types $\mathcal{S}^F_{\mathbb{BB}}$ and $\mathcal{S}^F_{\mathbb{I}^2\mathbb{O}^2}$ for the formations in Fig. 11(a) and (b), respectively. We remark, however, that the subformation $F_2\cup F_3$ is not rigid, violating the hypothesis of the previous work and, thus, the singularities sets $\mathcal{S}^F_{\mathbb{BB}}$ and $\mathcal{S}^F_{\mathbb{I}^2\mathbb{O}^2}$ are only a subset of the full set of singularities. In the case of Fig. 11(a), the formation is indeed generically bearing flexible (as determined by an analysis of the bearing rigidity matrix), and thus, the singularities are of little interest. In the case of Fig. 11(b), however, the formation is generically rigid and the analysis could be potentially useful. It may be recognized that the three rigid subformations are interconnected by only directed edges, and that in both the local singularity and the bi-partition subformation singularity analyzes, a frequent singularity of directed edge subgraphs is that all agents lie on a horizontal plane. We may, therefore, test and confirm numerically that if all six agents of the inner hexagon in Fig. 11(b) lie on a common horizontal plane, the formation has two singular DOF, while moving any single inner agent out of the plane restores rigidity. This, however, is not a rigorous analysis and could be missing many other singular configurations.

The singularity analysis of these types of formations could possibly be solved by fixing one of the three rigid subformations, and performing a kinematic analysis on the resulting virtual mechanism, similar to a multiplatform parallel robot. The analysis of these mechanisms with multiple closed kinematic loops without sharing a common ground link is currently an emerging topic in the robotics and kinematics community. Tools, such as screw theory, are augmented with the use of Assur graphs [58], however, even without accounting for the potentially expandable platform(s) in the virtual mechanism analysis, this is currently too complicated of an analysis to consider in this article and is left as an open axis of future research.

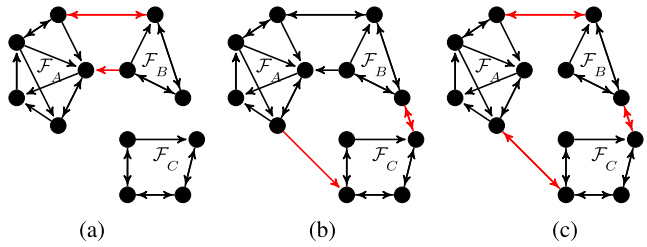

Fig. 12. Synthesis of a formation $\mathcal{F}_{ABC}$ with known singularities, from subformations $\mathcal{F}_A$, $\mathcal{F}_B$, and $\mathcal{F}_C$. The red edges are edges, which are added to join previously seperate subformations at a given step in the procedure. (a) Correct operation. (b) Correct operation. (c) Incorrect operation.

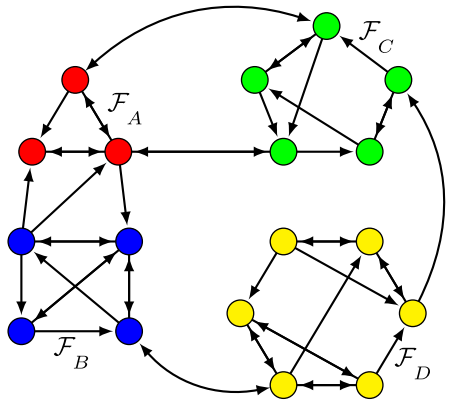

Fig. 13. Formation with a conservatively known set of singularities generated created by the combination of four rigid subformations $\mathcal{F}_A$, $\mathcal{F}_B$ $\mathcal{F}_C$ and $\mathcal{F}_D$ (separated by color). We remark that $\mathcal{F}_B$, $\mathcal{F}_C$, and $\mathcal{F}_D$ may be built in the manner currently being demonstrated.

VII. Design of Formations With Fully Known Singularities

As discussed in the previous section, the analysis of singularities for arbitrary formations remains computationally difficult and cannot be guaranteed to detect all singular conditions. It can be shown, however, that arbitrarily large formation graphs with conservatively known sets of singular conditions (i.e., a set guaranteed to encompass all singular, and possibly some nonsingular conditions) may be designed.

A. Methodology

To create a large formation for which we can guarantee that all singularities lie withing a known set of conditions, one must begin with two distinct intrinsically rigid formations (denoted $\mathcal{F}_A$ and $\mathcal{F}_B$) for which the singularities are well known. This is achievable for small formations composed of a basis of rigid loops (e.g., loops containing 3–4 agents with at least one or three $\mathbb{B}$ edges, respectively[3]) and if desired, "formation" may refer to a single agent or two agents joined by a $\mathbb{B}$ edge. Given that the singularities of the two formations ($\mathcal{S}_A$ and $\mathcal{S}_B$) are well known, and that adding graph edges further constrains both formations, the addition of any graph edges joining $\mathcal{F}_A$ to $\mathcal{F}_B$ will only contract $\mathcal{S}_A$ and $\mathcal{S}_B$. If the added graph edges are sufficient to make $\mathcal{F}_A$ and $\mathcal{F}_B$ into a single generically rigid formation $\mathcal{F}_{AB}$, the set of singularities of $\mathcal{F}_{AB}$ is necessarily a subset of the union of $\mathcal{S}_A$, $\mathcal{S}_B$ and the singularities exposed by bipartitioning $\mathcal{F}_{AB}$ between its two original components (denoted as $\mathcal{S}^F_{A/B}$)

$$\mathcal{S}_{AB} \subset \mathcal{S}^F_{A/B} \cup \mathcal{S}_A \cup \mathcal{S}_B. \tag{32}$$

In the example shown in Fig. 12(a), $\mathcal{S}^F_{A/B}$ is simply $\mathcal{S}^F_{\mathbb{BO}}$ and corresponds to the subformation partitioning exposed by cutting the red edges joining $\mathcal{F}_A$ and $\mathcal{F}_B$.

This combination of formations may then be repeated as many times as desired, so long as at every step the result is a rigid formation, and the singularities of the added formation are know. In Fig. 12(b), the connection of $\mathcal{F}_{AB}$ to $\mathcal{F}_C$ is a rigid operation (with the singularities $\mathcal{S}^F_{AB/C}$) and $\mathcal{S}_C$ is known, thus, the set of singularities for the formation is guaranteed to satisfy

$$\mathcal{S}_{ABC} \subset \mathcal{S}^F_{AB/C} \cup \mathcal{S}_{AB} \cup \mathcal{S}_C. \tag{33}$$

[3]This requirement can be confirmed by either a screw analysis or a numerical analysis of all ten possible 3–4 agent loops.

In the case of Fig. 12(c), however, we have no knowledge of the singularities from a tri-partition (see Section VI-D, using the notation here it would be $\mathcal{S}^F_{A/B/C}$), thus, even if we find some singularities of this formation, we cannot guarantee that all singularities lie within the set of those found.

An interesting extension of this singularity analysis by formation design is that it allows the analysis of formations with repeating structures, such as triangular lattices. In fact, as a triangular lattice may be formed by the ad infinitum addition of a new agent connected to two or more connected agents, the set of singularities will simply be a contraction of local singularities whenever a new agent is introduced.

B. Case Study: Singularity Analysis and Control of a 18-Agent Formation

To demonstrate the interest of this approach for the characterization of formation singularities, we consider the following case study: an 18-agent, 47-edge formation created from three, four, five, and six-agent rigid formations (see Fig. 13). First $\mathcal{F}_A$ and $\mathcal{F}_B$ are connected to form $\mathcal{F}_{AB}$ and $\mathcal{F}_C$ is added to create $\mathcal{F}_{ABC}$ (the order of these two steps is interchangeable, as they both rigidly connect to $\mathcal{F}_A$). Finally, $\mathcal{F}_D$ is added to create the full formation $\mathcal{F}_{ABCD}$. The undirected graph of this formation has 32 edges.

We first analyze the singularities of this formation and we then use the known conditions of singularity in order to develop a singularity-avoidance controller using the information obtained with the singularity analysis.

1) Singularity Analysis: The set of singularities for this formation can be fully guaranteed to lie within a known set of conditions as previously explained. This set encompasses the local singularities of all agents, and some additional subformation singularities. Three of the subformation singularities correspond to the combination of rigid formations ($\mathcal{S}^F_{A/B}$, $\mathcal{S}^F_{AB/C}$, and $\mathcal{S}^F_{ABC/D}$) while other subformation singularities are intrinsic to the individual formations. Formations $\mathcal{F}_B$, $\mathcal{F}_C$, and $\mathcal{F}_D$ can in fact be created by the method, we are describing, and

TABLE IV
NUMBER AND TYPES OF SINGULARITIES IN DIFFERENT PARTS OF THE FORMATION SHOWN IN FIG. 13

Component	Number and types of $\mathcal{S}^L$	Number and types of $\mathcal{S}^F$
$\mathcal{S}_A$	3 types of local sing.: • $\mathcal{S}^L_{\mathbb{BO}}$ with $\mathbb{B}$: $\mathcal{A}_1 \leftrightarrow \mathcal{A}_3$, $\mathbb{O}$: $\mathcal{A}_1 \rightarrow \mathcal{A}_2$; • $\mathcal{S}^L_{\mathbb{BI}}$ with $\mathbb{B}$: $\mathcal{A}_2 \leftrightarrow \mathcal{A}_3$, $\mathbb{I}$: $\mathcal{A}_2 \leftarrow \mathcal{A}_1$; • $\mathcal{S}^L_{\mathbb{BB}}$ with $\mathbb{B}$: $\mathcal{A}_3 \leftrightarrow \mathcal{A}_1$, $\mathcal{A}_3 \leftrightarrow \mathcal{A}_2$	N/A
$\mathcal{S}_B$	4 types of local sing.: • $\mathcal{S}^L_{\mathbb{BOI}}$ with $\mathbb{B}$: $\mathcal{A}_4 \leftrightarrow \mathcal{A}_5$, $\mathbb{O}$: $\mathcal{A}_4 \rightarrow \mathcal{A}_7$, $\mathbb{I}$: $\mathcal{A}_4 \leftarrow \mathcal{A}_6$; • $\mathcal{S}^L_{\mathbb{BBB}}$ with $\mathbb{B}$: $\mathcal{A}_5 \leftrightarrow \mathcal{A}_4$, $\mathbb{B}$: $\mathcal{A}_5 \leftrightarrow \mathcal{A}_6$, $\mathbb{B}$: $\mathcal{A}_5 \leftrightarrow \mathcal{A}_7$; • $\mathcal{S}^L_{\mathbb{BOI}}$ with $\mathbb{B}$: $\mathcal{A}_6 \leftrightarrow \mathcal{A}_5$, $\mathbb{O}$: $\mathcal{A}_6 \rightarrow \mathcal{A}_4$, $\mathbb{I}$: $\mathcal{A}_6 \leftarrow \mathcal{A}_7$; • $\mathcal{S}^L_{\mathbb{BOI}}$ with $\mathbb{B}$: $\mathcal{A}_7 \leftrightarrow \mathcal{A}_5$, $\mathbb{O}$: $\mathcal{A}_7 \rightarrow \mathcal{A}_6$, $\mathbb{I}$: $\mathcal{A}_7 \leftarrow \mathcal{A}_4$.	N/A
$\mathcal{S}^F_{A/B}$	N/A	1 type of formation sing.: $\mathcal{S}^F_{\mathbb{IOO}}$ with $\mathbb{I}$: $\mathcal{A}_5 \leftarrow \mathcal{A}_3$ $\mathbb{O}$: $\mathcal{A}_4 \rightarrow \mathcal{A}_2$ $\mathbb{O}$: $\mathcal{A}_4 \rightarrow \mathcal{A}_3$
$\mathcal{S}_C$	5 types of local sing.: • $\mathcal{S}^L_{\mathbb{BOI}}$ with $\mathbb{B}$: $\mathcal{A}_8 \leftrightarrow \mathcal{A}_{12}$, $\mathbb{O}$: $\mathcal{A}_8 \rightarrow \mathcal{A}_{11}$, $\mathbb{I}$: $\mathcal{A}_8 \leftarrow \mathcal{A}_9$; • $\mathcal{S}^L_{\mathbb{BO}}$ with $\mathbb{B}$: $\mathcal{A}_9 \leftrightarrow \mathcal{A}_{10}$, $\mathbb{O}$: $\mathcal{A}_9 \rightarrow \mathcal{A}_8$; • $\mathcal{S}^L_{\mathbb{BOI}}$ with $\mathbb{B}$: $\mathcal{A}_{10} \leftrightarrow \mathcal{A}_9$, $\mathbb{O}$: $\mathcal{A}_{10} \rightarrow \mathcal{A}_{12}$, $\mathbb{I}$: $\mathcal{A}_{10} \leftarrow \mathcal{A}_{11}$; • $\mathcal{S}^L_{\mathbb{OII}}$ with $\mathbb{O}$: $\mathcal{A}_{11} \rightarrow \mathcal{A}_{10}$, $\mathbb{I}$: $\mathcal{A}_{11} \leftarrow \mathcal{A}_8$, $\mathbb{I}$: $\mathcal{A}_{11} \leftarrow \mathcal{A}_{12}$; • $\mathcal{S}^L_{\mathbb{BOI}}$ with $\mathbb{B}$: $\mathcal{A}_{12} \leftrightarrow \mathcal{A}_8$, $\mathbb{O}$: $\mathcal{A}_{12} \rightarrow \mathcal{A}_{11}$, $\mathbb{I}$: $\mathcal{A}_{12} \leftarrow \mathcal{A}_{10}$.	N/A
$\mathcal{S}^F_{AB/C}$	N/A	1 type of formation sing.: $\mathcal{S}^F_{\mathbb{BB}}$ with $\mathbb{B}$: $\mathcal{A}_1 \leftrightarrow \mathcal{A}_8$ $\mathbb{B}$: $\mathcal{A}_3 \leftrightarrow \mathcal{A}_{11}$
$\mathcal{S}_D$	6 types of local sing.: • $\mathcal{S}^L_{\mathbb{BB}}$ with $\mathbb{B}$: $\mathcal{A}_{13} \leftrightarrow \mathcal{A}_{14}$, $\mathbb{B}$: $\mathcal{A}_{13} \leftrightarrow \mathcal{A}_{18}$; • $\mathcal{S}^L_{\mathbb{BI}}$ with $\mathbb{B}$: $\mathcal{A}_{14} \leftrightarrow \mathcal{A}_{13}$, $\mathbb{I}$: $\mathcal{A}_{14} \leftarrow \mathcal{A}_{18}$; • $\mathcal{S}^L_{\mathbb{BB}}$ with $\mathbb{B}$: $\mathcal{A}_{15} \leftrightarrow \mathcal{A}_{16}$, $\mathbb{B}$: $\mathcal{A}_{15} \leftrightarrow \mathcal{A}_{17}$; • $\mathcal{S}^L_{\mathbb{BB}}$ with $\mathbb{B}$: $\mathcal{A}_{16} \leftrightarrow \mathcal{A}_{15}$, $\mathbb{B}$: $\mathcal{A}_{16} \leftrightarrow \mathcal{A}_{17}$; • $\mathcal{S}^L_{\mathbb{BB}}$ with $\mathbb{B}$: $\mathcal{A}_{17} \leftrightarrow \mathcal{A}_{15}$, $\mathbb{B}$: $\mathcal{A}_{17} \rightarrow \mathcal{A}_{16}$; • $\mathcal{S}^L_{\mathbb{BO}}$ with $\mathbb{B}$: $\mathcal{A}_{18} \leftrightarrow \mathcal{A}_{13}$, $\mathbb{O}$: $\mathcal{A}_{18} \rightarrow \mathcal{A}_{14}$.	1 type of formation sing.: $\mathcal{S}^F_{\mathbb{IOO}}$ with $\mathbb{I}$: $\mathcal{A}_{17} \leftarrow \mathcal{A}_{18}$ $\mathbb{O}$: $\mathcal{A}_{16} \rightarrow \mathcal{A}_{13}$ $\mathbb{O}$: $\mathcal{A}_{15} \rightarrow \mathcal{A}_{14}$
$\mathcal{S}^F_{ABC/D}$	N/A	1 type of formation sing.: $\mathcal{S}^F_{\mathbb{BO}}$ with $\mathbb{B}$: $\mathcal{A}_6 \leftrightarrow \mathcal{A}_{16}$ $\mathbb{O}$: $\mathcal{A}_{14} \rightarrow \mathcal{A}_9$
Total	**18**	**4**

thus, we are able to guarantee that there is only one single subformation singularity in $\mathcal{F}_D$. We can, therefore, guarantee that all singularities are encompassed by 22 sets of singularity types corresponding to 18 local sets, three intersubformation sets, and one intrasubformation set (see Table IV). It should be mentioned here that the singularity sets can be automatically detected by a program as long as we know how the formation is built, as shown in the MATLAB code provided as additional material to this article.

These set of singularities are then translated into geometric conditions in the Tables V and VI: removing the redundant conditions, 17 geometric configurations lead to local singularities, while 27 configurations correspond to subformation singularities. All conditions leading to local singularities are

TABLE V
GEOMETRIC CONDITIONS LEADING TO LOCAL SINGULARITIES OF THE FORMATION SHOWN IN FIG. 13

Component	$\mathcal{S}^L$
$\mathcal{S}_A$	• $\mathcal{A}_1$, $\mathcal{A}_2$, $\mathcal{A}_3$ aligned • $\mathcal{A}_2$, $\mathcal{A}_3$ on a vertical line.
$\mathcal{S}_B$	• $\mathcal{A}_4$, $\mathcal{A}_5$, $\mathcal{A}_6$, $\mathcal{A}_7$ aligned • $\mathcal{A}_4$, $\mathcal{A}_5$, $\mathcal{A}_7$ on a vertical line • $\mathcal{A}_4$, $\mathcal{A}_5$, $\mathcal{A}_6$ on a vertical line • $\mathcal{A}_5$, $\mathcal{A}_6$, $\mathcal{A}_7$ on a vertical line.
$\mathcal{S}_C$	• $\mathcal{A}_8$, $\mathcal{A}_9$, $\mathcal{A}_{11}$, $\mathcal{A}_{12}$ aligned • $\mathcal{A}_8$, $\mathcal{A}_{11}$, $\mathcal{A}_{12}$ on a vertical line • $\mathcal{A}_8$, $\mathcal{A}_9$, $\mathcal{A}_{10}$ aligned • $\mathcal{A}_9$, $\mathcal{A}_{10}$, $\mathcal{A}_{11}$, $\mathcal{A}_{12}$ aligned • $\mathcal{A}_9$, $\mathcal{A}_{10}$, $\mathcal{A}_{12}$ on a vertical line • $\mathcal{A}_8$, $\mathcal{A}_{10}$, $\mathcal{A}_{11}$, $\mathcal{A}_{12}$ aligned • $\mathcal{A}_8$, $\mathcal{A}_{10}$, $\mathcal{A}_{11}$ on a vertical line • $\mathcal{A}_{10}$, $\mathcal{A}_{12}$ on a vertical line.
$\mathcal{S}_D$	• $\mathcal{A}_{13}$, $\mathcal{A}_{14}$, $\mathcal{A}_{18}$ aligned • $\mathcal{A}_{13}$, $\mathcal{A}_{14}$ on a vertical line • $\mathcal{A}_{15}$, $\mathcal{A}_{16}$, $\mathcal{A}_{17}$ aligned.
Total	**17 conditions**

TABLE VI
GEOMETRIC CONDITIONS LEADING TO SUBFORMATION SINGULARITIES OF THE FORMATION SHOWN IN FIG. 13

Component	$\mathcal{S}^F$
$\mathcal{S}^F_{A/B}$	Line $\mathcal{L}_1$ contains $\mathcal{A}_3$, $\mathcal{A}_5$, Line $\mathcal{L}_2$ contains $\mathcal{A}_3$, $\mathcal{A}_4$, Line $\mathcal{L}_3$ contains $\mathcal{A}_2$, $\mathcal{A}_4$: • $\mathcal{L}_1$, $\mathcal{L}_2$ and $\mathcal{L}_3$ intersect • $\mathcal{L}_1$, $\mathcal{L}_2$ and $\mathcal{L}_3$ parallel • $\mathcal{L}_1$, $\mathcal{L}_2$ and $\mathcal{L}_3$ vertical and superposed • $\mathcal{L}_1$, $\mathcal{L}_2$ vertical and superposed, with $\mathcal{A}_3$ on $\mathcal{L}_1$ • $\mathcal{L}_1$, $\mathcal{L}_3$ vertical and superposed, with $\mathcal{A}_2$ on $\mathcal{L}_1$ • $\mathcal{L}_2$ vertical & $\mathcal{A}_5$, $\mathcal{A}_3$ on $\mathcal{L}_2$ • $\mathcal{L}_3$ vertical & $\mathcal{A}_5$, $\mathcal{A}_2$ on $\mathcal{L}_3$ • $\mathcal{A}_5$ and $\mathcal{A}_2$ or $\mathcal{A}_3$ on the same vertical line • All agents $\mathcal{A}_2$, $\mathcal{A}_3$, $\mathcal{A}_4$, $\mathcal{A}_5$ lie on a common horizontal plane • Lines $\mathcal{L}_2$ and $\mathcal{L}_3$ are horizontal and the intersection of two horizontal lines passing through the projections of $\mathcal{A}_2$ and $\mathcal{A}_3$ in an horizontal plane is on the vertical axis passing through $\mathcal{A}_5$.
$\mathcal{S}^F_{AB/C}$	Line $\mathcal{L}_1$ contains $\mathcal{A}_1$, $\mathcal{A}_8$, Line $\mathcal{L}_2$ contains $\mathcal{A}_3$, $\mathcal{A}_{11}$: • $\mathcal{L}_1$ and $\mathcal{L}_2$ intersect • $\mathcal{L}_1$ and $\mathcal{L}_2$ parallel • $\mathcal{L}_1$ and $\mathcal{L}_2$ vertical and superposed.
$\mathcal{S}_D$	Line $\mathcal{L}_1$ contains $\mathcal{A}_{17}$, $\mathcal{A}_{18}$, Line $\mathcal{L}_2$ contains $\mathcal{A}_{16}$, $\mathcal{A}_{13}$, Line $\mathcal{L}_3$ contains $\mathcal{A}_{15}$, $\mathcal{A}_{14}$: • $\mathcal{L}_1$, $\mathcal{L}_2$ and $\mathcal{L}_3$ intersect • $\mathcal{L}_1$, $\mathcal{L}_2$ and $\mathcal{L}_3$ parallel • $\mathcal{L}_1$, $\mathcal{L}_2$ and $\mathcal{L}_3$ vertical and superposed • $\mathcal{L}_1$, $\mathcal{L}_2$ vertical and superposed, with $\mathcal{A}_{14}$ on $\mathcal{L}_1$ • $\mathcal{L}_1$, $\mathcal{L}_3$ vertical and superposed, with $\mathcal{A}_{13}$ on $\mathcal{L}_1$ • $\mathcal{L}_2$ vertical & $\mathcal{A}_{17}$, $\mathcal{A}_{14}$ on $\mathcal{L}_2$ • $\mathcal{L}_3$ vertical & $\mathcal{A}_{17}$, $\mathcal{A}_{13}$ on $\mathcal{L}_3$ • $\mathcal{A}_{17}$ and $\mathcal{A}_{13}$ or $\mathcal{A}_{14}$ on the same vertical line • All agents $\mathcal{A}_{13}$, $\mathcal{A}_{14}$, $\mathcal{A}_{15}$, $\mathcal{A}_{16}$, $\mathcal{A}_{17}$, $\mathcal{A}_{18}$ lie on a common horizontal plane • Lines $\mathcal{L}_2$ and $\mathcal{L}_3$ are horizontal and the intersection of two horizontal lines passing through the projections of $\mathcal{A}_{13}$ and $\mathcal{A}_{14}$ in an horizontal plane is on the vertical axis passing through $\mathcal{A}_{17}$.
$\mathcal{S}^F_{ABC/D}$	Line $\mathcal{L}_1$ contains $\mathcal{A}_6$, $\mathcal{A}_{16}$, Line $\mathcal{L}_2$ contains $\mathcal{A}_9$, $\mathcal{A}_{14}$: • $\mathcal{L}_1$ and $\mathcal{L}_2$ intersect • $\mathcal{L}_1$ and $\mathcal{L}_2$ parallel • $\mathcal{L}_1$ and $\mathcal{L}_2$ vertical and superposed. • $\mathcal{L}_1$ vertical and contains $\mathcal{A}_9$.
Total	**27 conditions**

due to alignments of at least three agents or to some agents lying on a vertical line. Configurations leading to subformation singularities may be due to more complex geometric constraints, especially singularities associated with $\mathbb{IOO}$ connections between subformations.

It should be mentioned that we tested all these configurations of singularity, by assigning to the positions of the agent some numerical values corresponding to geometric configurations shown in Tables V and VI: all cases correspond to a loss of rank of the bearing rigidity matrix.

2) Singularity-Avoidance Controller: Here, we show how our singularity analysis may serve to develop a singularity-avoidance controller. For this, we take inspiration from the works [32], [33] in which controllers for rigidity maintenance taking into account the singularity of the rigidity matrix are proposed. In these papers, singularities of the rigidity matrix are avoided by paying attention to its minimal singular value λ_6, which is forced to stay greater than a given threshold $\lambda_{\min}$: For this, a penalty (potential) function V is introduced which tends to infinity when λ_6 comes close to $\lambda_{\min}$ and to zero when $\lambda_6 \gg \lambda_{\min}$. The controller is set up so that it minimizes both the potential function V and the bearing measurement error. However, the computation of the singular value λ_6 requires the knowledge of the full formation configuration by all agents. In order to overpass this difficulty, a strategy based on consensus theory is implemented in [33], which allows each agent to have a distributed estimation of λ_6. The implementation of the distributed estimation of the rigidity eigenvalue and eigenvector requires a tenth-order dynamic estimator including several interconnected components for each agent that are listed here.

1) Estimation of a common reference frame or estimation of the relative position with respect to a common reference point, shared by all agents.
2) Estimation of the rigidity eigenvector using the power iteration method summarized in [33] where some constant gains constraints have to be ensured.
3) Design of three proportional integral-consensus filters.

In their work, the integration of the relative position estimator, the rigidity eigenvalue estimator, and the gradient controller leads to a highly nonlinear dynamics for which a proof analysis is not provided. The approach exploited the typical time-scale separation argument commonly found in robotics applications. The estimator dynamics is assumed *fast enough* with respect to the robot motion. Some experimental results illustrated the satisfactory performance including the accuracy of the estimation strategy.

Here, we propose to develop a singularity-avoidance controller, which does not require this general estimation of λ_6 by all agents. This approach exploits the geometric conditions given in Tables V and VI, which need the sharing of information with no more than three neighbors for most of singularity condition computations. For all conditions due to line intersection, parallelism, or superposition, it is always possible to define indices bounded between 0 and 1, 0 being the condition of fulfillment of the geometric condition. For instance, an index for the intersection of two lines could be defined as what follows: Let us define three lines $\mathcal{L}_1$, $\mathcal{L}_2$, and $\mathcal{L}_3$ with Plücker coordinates

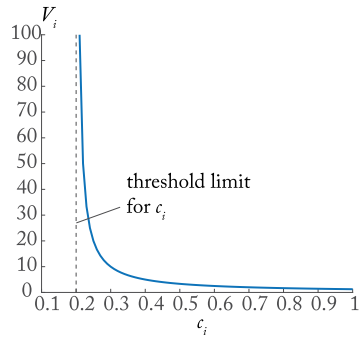

Fig. 14. Example of potential function $V_i(c_i)$.

$\mathcal{L}_i = [\mathbf{u}_i^T \ \mathbf{h}_i^T]^T$, with $\mathbf{u}_i$ the vector defining the direction of the line, and $\mathbf{h}_i = \overrightarrow{OM_i} \times \mathbf{u}_i$ where the point M_i belongs to the line $\mathcal{L}_i$ and O is any arbitrary point. Thus, $\mathbf{h}_i$ is nothing else than the moment of $\mathbf{u}_i$ computed in O. Then, if $\mathcal{L}_1$, $\mathcal{L}_2$, and $\mathcal{L}_3$ share a common point, their moments $\mathbf{h}_1$, $\mathbf{h}_2$, $\mathbf{h}_3$ are linearly dependent, i.e.,

$$\mathbf{h}_1^T(\mathbf{h}_2 \times \mathbf{h}_3) = 0. \tag{34}$$

This criterion can be bounded between 0 and 1 by modifying it as follows:

$$c = \left| \frac{\mathbf{h}_1^T(\mathbf{h}_2 \times \mathbf{h}_3)}{\|\mathbf{h}_1\|\|\mathbf{h}_2 \times \mathbf{h}_3\|} \right|. \tag{35}$$

Bounding the criterions between 0 and 1 is of interest, because it is, thus, simpler to define a threshold value characterizing an acceptable "distance" to singularity. However, this is not feasible for all singularity criterions. For instance, for defining the coplanarity of points of four points, it is more difficult to do so, but a zero still means that the condition is achieved. It should be noted that the same problem arises when controlling the smallest eigenvalue λ_6 of the bearing rigidity matrix, like it is done in [33] and [32]. In particular, it is difficult to define what should be a good threshold $\lambda_{\min}$ for large formations, and this question is still an open issue.

So we define 44 singularity criterions based on the conditions provided in Tables V and VI: These indices can be computed as shown in the MATLAB code given as additional material. Let us denote as $\mathbf{c}$ the vector stacking all the numerical values associated with these 44 singularity criterions.

For each of the 44 singularity criterions grouped in the vector $\mathbf{c}$, we associate a potential function V_i corresponding to the component i of $\mathbf{c}$ like it was done in [33]: The function V_i takes a high value when c_i is close to its user-defined threshold $c_{\min}$, and a zero value when $c_i \gg c_{\min}$. Note that the threshold $c_{\min}$ can be the same for all singularity conditions. Examples of such potential functions are provided in Fig. 14. All these potential functions are grouped into the vector $\mathbf{v}$.

Finally, we define global potential function V such that

$$V = \alpha \mathbf{e}^T\mathbf{e} + \gamma \mathbf{v}^T\mathbf{W}_v\mathbf{v} \tag{36}$$

where

1) $\mathbf{e} = \boldsymbol{\beta} - \boldsymbol{\beta}^d$ is the error between the actual bearings $\boldsymbol{\beta}$ and their desired values $\boldsymbol{\beta}^d$;
2) $\mathbf{W}_v$ is a weight matrix which forces the drones to keep a desired interdistance $d_{\min}$ between them; In our simulations, $d_{\min} = 0.6$ m;
3) α and γ are two gains to be tuned in order to set more importance between trying to reach the desired bearings and avoiding to reach a singularity. γ can be set to 0 if we decide to cancel the effect of the singularity-avoidance terms inside the potential function V.

Then, in order to control the fleet, we apply a standard gradient-descent-based strategy, which allows the minimization of the potential function V [32], [33]. Note that more advanced strategies based on quadratic programming and dedicated to barriers certificates could be used [59]. However, they are left as perspectives of our work.

An illustration of this approach is shown in Figs. 15 and 16. In order to highlight our *proof-of-concept* by simulations, we consider that all agents perfectly know the position of all the others. Distributed control strategies could be defined, but this is out of the scope of this work, and they are left as research perspectives. It should, however, be noted that, for all the computations required for the definition of these indices, each agent must share its position information with no more than five other agents. Even, for most of indices, this information sharing number is limited to three neighbors, compared with the approaches [32], [33] for which all agents should have an estimation of the pose of all the others.

The drone formation is initialized in a random configuration shown in Fig. 15(a). We ask the formation to reach a configuration in which there is a singularity.

1) First, by putting the gain γ at 0 ($\alpha = 25$), we cancel the singularity avoidance terms. We see in Fig. 15 that the formation is going into the singularity: At the end of the simulation, the smallest eigenvalue λ_6 is null, as well as one of the indices c_i, while the error on the bearing measurements is null.
2) Then, we conserve the singularity avoidance terms ($\alpha = 50$, $\gamma = 5000$). We see in Fig. 16 that the formation is no more going into the singularity: At the end of the simulation, the smallest eigenvalue λ_6 is different from 0, as well as all the indices c_i, while the error on the bearing measurements is no more null, which is normal as this configuration cannot be attained without having a singular formation.

These results properly illustrate how our work can be used in order to define a singularity-avoidance controller with the knowledge we brought on singularity of formations.

In order to conclude this section, we should mention that the main limits of singularity analysis through formation design is the fact that some rigid formations (as explained in Section VI-D) are excluded, and that the formations are required to have more edges than strictly necessary. Despite this, all formations that are created using this methodology are guaranteed to be nonsingular outside of the known set of geometric conditions. In addition to providing human-interpretable information on the

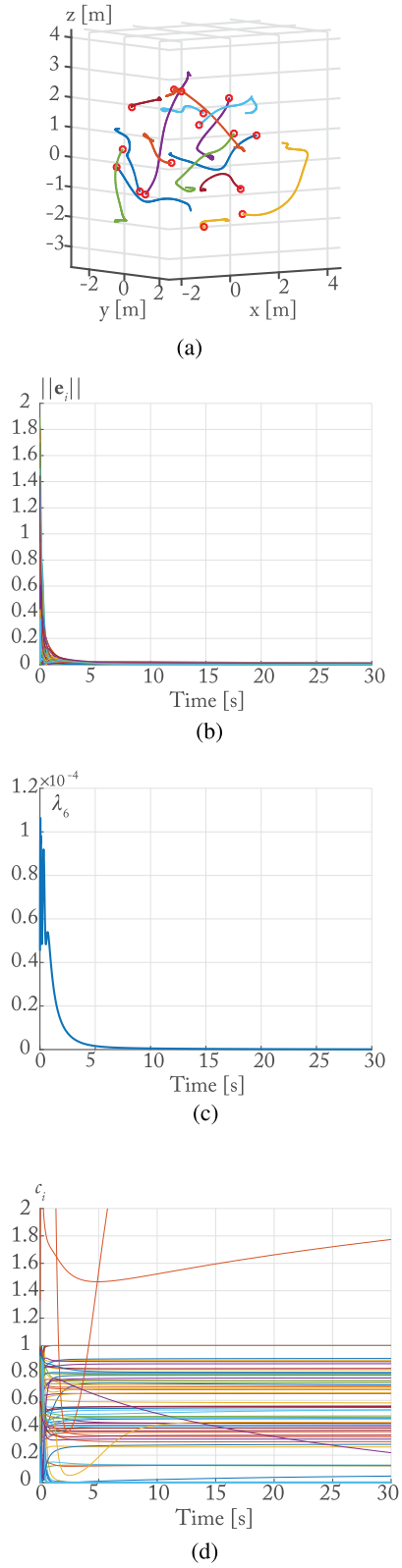

Fig. 15. Evolution of the 18-agent fleet with no singularity-avoidance controller. (a) Initial configuration of the fleet (agents are represented by red circle) and their trajectory. (b) Evolution of the bearing errors. (c) Evolution of the smallest singular value λ_6. (d) Evolution of the geometric conditions c_i.

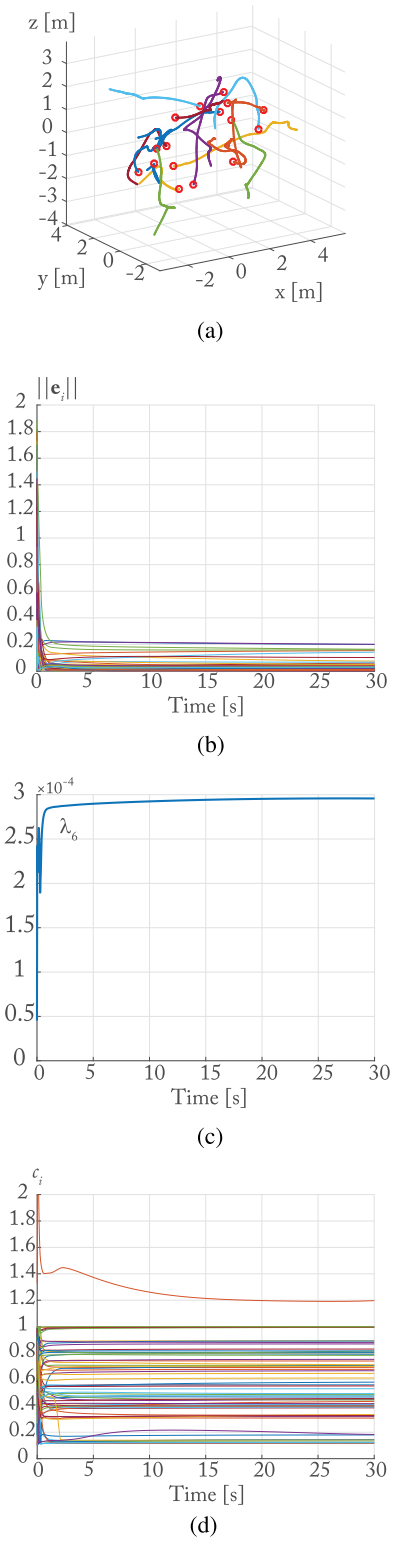

Fig. 16. Evolution of the 18-agent fleet with a singularity avoidance controller based on our geometric criterions. (a) Initial configuration of the fleet (agents are represented by red circle) and their trajectory. (b) Evolution of the bearing errors. (c) Evolution of the smallest singular value λ_6. (d) Evolution of the geometric conditions c_i.

conditions of singularities, these conditions could be included as constraints in onboard controllers, as shown in this last section. Beyond its application in formation design and control, it also has practical relevance in the analysis of singularities appearing in large formations *if* one is able to identify smaller intrinsically rigid subformations within the graph, or when multiple pre-existing formations merge in real-time operation.

VIII. Conclusion

This article presented a novel perspective on the geometric analysis of singular embeddings of bearing graphs, which has practical relevance in the decentralized formation control of multirobot systems. Until now, the analysis of singular embeddings causing the framework of a generically rigid bearing graph to become flexible has only been solved for some small graphs, and has not been not systematically studied.

A. Methods and Results

By applying the "hidden robot" methodology to perform a kinematic analysis of substructures of the graph, we have shown that it is feasible to determine an extensive set geometric conditions for which large frameworks on the $\mathbb{R}^3 \times \mathcal{S}^1$ manifold become singular (i.e., lose rigidity). Furthermore, we have demonstrated how to design formations of unbounded size with a fully known set of singular conditions such that by operating outside this set of conditions, the framework is guaranteed to be rigid.

We have also shown that the method presented in this article may be used for guaranteeing the performance of decentralized bearing formation controllers for which the property of rigidity is necessary to ensure convergence. The results of this article may be applied directly to formations of quadrotor-like UAVs, surface-based mobile robots (moving on the $\mathrm{SE}(2)$ or other submanifolds of $\mathbb{R}^3 \times \mathcal{S}^1$) or a combination thereof.

B. Open Perspectives

This article only treated the case of singularities on the $\mathbb{R}^3 \times \mathcal{S}^1$ manifold, corresponding to quadrotors and ground-based mobile robots. The same graph decomposition strategy could be extended to the $\mathrm{SE}(3)$ manifold in order to be applied to formations of omni-directional UAVs or satellites, and for solving network localization problems for bearing sensors in 6 DOF. Furthermore, this work only considers bearing formations, and could be extended to distance or mixed bearing-distance rigidity problems.

We also expect to solve certain problems that we left unsolved, such as the $k > 2$-partition subformation singularities, and finding minimum sets of unique geometric conditions to avoid redundancy among singular configurations.

Appendix A
Example of Application of the Screw Theory: the RRR Mechanism

A. Wrench Set Computation of an RR Serial Chain

To demonstrate the concept of reciprocal screws, in Fig. 17(a) is shown an example of a serial kinematic chain composed of

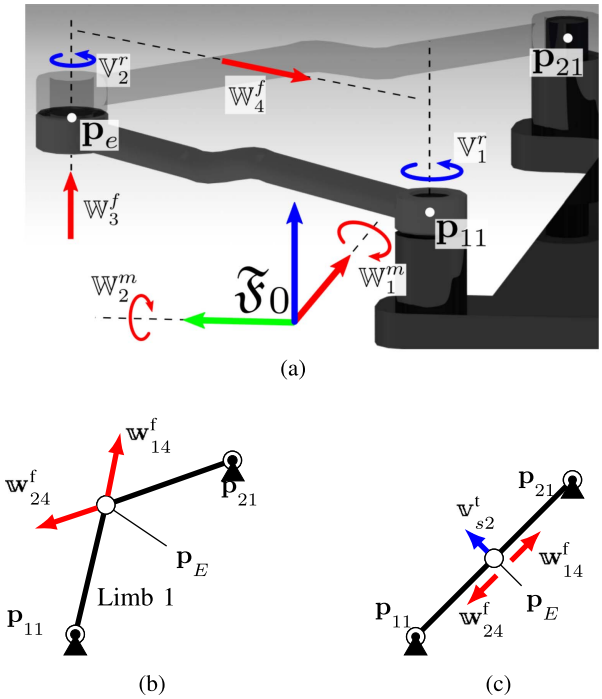

Fig. 17. Representation of rigid and singular configurations of a planar RRR parallel mechanism composed of two RR limbs. Revolute joints containing a dot are pinned to the ground link. (a) Isometric view of an RRR parallel linkage with the twists (in blue) and wrenches (in red) of Limb 1 being labeled. (b) Top view of an RRR mechanism in a rigid configuration. (c) Top view of an RRR mechanism in a singular configuration.

two revolute (denoted by "R") joints at points with coordinates $\mathbf{p}_{11}\ (=\mathbf{p}_1)$ and $\mathbf{p}_e\ (=\mathbf{p}_2)$ (forming an RR chain) connected by a rigid link of unit length. The axes of both R joints are directed along $\mathbf{z}_0$. The twist set of the serial chain is, therefore

$$\mathcal{T}_{\text{RR}} = \{\mathbb{v}_1^{\text{r}}(\mathbf{z}_0, \mathbf{p}_1),\ \mathbb{v}_2^{\text{r}}(\mathbf{z}_0, \mathbf{p}_2)\} \tag{37}$$

where $\mathbf{p}_1$ and $\mathbf{p}_2$ are the positions of the two R joints in $\mathfrak{F}_0$. The rank of the twist set can be determined by evaluating a matrix where every column is a twist

$$\mathcal{T}_{\text{RR}} = \begin{bmatrix}\mathbb{v}_1^{\text{r}} & \mathbb{v}_2^{\text{r}}\end{bmatrix} = \begin{bmatrix}(\mathbf{z}_0 \times \mathbf{p}_1) & (\mathbf{z}_0 \times \mathbf{p}_2)\\ \mathbf{z}_0 & \mathbf{z}_0\end{bmatrix}$$
$$= \begin{bmatrix}-p_{1y} & -p_{2y}\\ p_{1x} & p_{2x}\\ 0 & 0\\ 0 & 0\\ 0 & 0\\ 1 & 1\end{bmatrix} \tag{38}$$

where p_{ix} and p_{iy} are the x and y components of $\mathbf{p}_i$. It can clearly be seen that as long as the two points do not share a common axis $\mathbf{z}_0$, the rank of the twist set is 2. The degeneration of the serial chain twist set is in fact a type of singularity but is not relevant in the context of this article.

Applying the reciprocity conditions (13), we can find the reciprocal wrench set calculated and expressed in $\mathfrak{F}_0$ as

$$\mathcal{W}_{\text{RR}} = \{\mathbb{w}_1^{\text{m}}(\mathbf{x}_0), \mathbb{w}_2^{\text{m}}(\mathbf{y}_0), \mathbb{w}_3^{\text{f}}(\mathbf{z}_0, \mathbf{p}_2), \mathbb{w}_4^{\text{f}}(\mathbf{p}_{12}, \mathbf{p}_2)\} \tag{39}$$

with $\mathbf{p}_{12} = \mathbf{p}_2 - \mathbf{p}_1$, which like the twist set, may be expanded to

$$\mathcal{W}_{\text{RR}} = \begin{bmatrix}\mathbf{0} & \mathbf{0} & \mathbf{z}_0 & \mathbf{p}_{12}\\ \mathbf{x}_0 & \mathbf{y}_0 & \mathbf{z}_0 \times \mathbf{p}_2 & \mathbf{p}_{12} \times \mathbf{p}_2\end{bmatrix}$$
$$= \begin{bmatrix}0 & 0 & 0 & p_{12x}\\ 0 & 0 & 0 & p_{12y}\\ 0 & 0 & 1 & 0\\ 1 & 0 & -p_{2y} & 0\\ 0 & 1 & p_{2x} & 0\\ 0 & 0 & 0 & \theta\end{bmatrix} \tag{40}$$

where $\theta = p_{12x}p_{2y} - p_{12y}p_{2x}$. This wrench set contains two pure moments $\mathbb{w}_1^{\text{m}}(\mathbf{x}_0)$ and $\mathbb{w}_2^{\text{m}}(\mathbf{y}_0)$, which prevent the system to rotate around the axes $\mathbf{x}_0$ and $\mathbf{y}_0$ and two pure forces $\mathbb{w}_3^{\text{f}}(\mathbf{z}_0, \mathbf{p}_2)$, $\mathbb{w}_4^{\text{f}}(\mathbf{p}_{12}, \mathbf{p}_2)$, which prevent to translate along the directions $\mathbf{z}_0$ and $\mathbf{p}_{12}$.

B. Wrench Set Computation of an RRR Closed-Loop Mechanism and Singularity Analysis

Let us now consider the full RRR closed-loop mechanism shown in Fig. 17. For creating this mechanism, two serial RR chains (or limbs) as shown in Fig. 17(a) are connected in parallel, forming the closed-loop RRR mechanisms in Fig. 17(b)–(c). The first revolute joint of limb i is fixed to a grounded position $\mathbf{p}_{i1}$ (denoted by a dot in the figures), and the second revolute joints are joined together at a common point E at position $\mathbf{p}_E$. As explained before, each limb $i \in 1, 2$ exerts a set of wrenches $\mathcal{W}_{\text{RR}i}$, shown in (39), constraining point E resulting in the closed-loop wrench set

$$\mathcal{W}_{\text{RRR}} = \mathcal{W}_{\text{RR1}} \cup \mathcal{W}_{\text{RR2}} \tag{41}$$

that constrains possible twists of E in SE(3). Note that while this planar mechanism moves on the SE(2) manifold, a wrench set in SE(3) is required to constrain its motion to the SE(2) manifold (it was also true for the previous RR chain). The first three wrenches [$\mathbb{w}_1^{\text{m}}$, $\mathbb{w}_2^{\text{m}}$, and $\mathbb{w}_3^{\text{f}}$ from (39)] in $\mathcal{W}_{\text{RR}i}$ are identical for both limbs, and the duplicate columns can be eliminated when representing $\mathcal{W}_{\text{RRR}}$ as the matrix

$$\mathcal{W}_{\text{RRR}} = \begin{bmatrix}0 & 0 & 0 & p_{Ex} - p_{11x} & p_{Ex} - p_{21x}\\ 0 & 0 & 0 & p_{Ey} - p_{11y} & p_{Ey} - p_{21y}\\ 0 & 0 & 1 & 0 & 0\\ 1 & 0 & -p_{2y} & 0 & 0\\ 0 & 1 & p_{2x} & 0 & 0\\ 0 & 0 & 0 & \theta_1 & \theta_2\end{bmatrix} \tag{42}$$

where $\theta_i = p_{i1x}p_{Ey} - p_{i1y}p_{Ex}$.

The reader will remark that $\mathcal{W}_{\text{RRR}}$ can have at most a rank of 5 in a generic configuration [see Fig. 17(b)]. This corresponds to

a perpetual singular twist[4] $\mathbb{v}^{\mathrm{r}}_{s1}(\mathbf{z}_0, \mathbf{p}_e)$, which correspond to a rotation of point E about the $\mathbf{z}_0$ axis. A singular configuration of $\mathcal{W}_{\mathrm{RRR}}$ [see Fig. 17(c)] occurs when the last two columns ($\mathbb{w}^{\mathrm{f}}_{14}$ and $\mathbb{w}^{\mathrm{f}}_{24}$) become linearly dependant: then rank $(\mathcal{W}_{\mathrm{RRR}}) = 4$. When all revolute joint centers are aligned, like in Fig. 17(c), then a singular twist $\mathbb{v}^{\mathrm{t}}_{s2}(\mathbf{p}_E - \mathbf{p}_{11}, \mathbf{p}_E)$, reciprocal to all wrenches in $\mathcal{W}_{\mathrm{RRR}}$, exists.

REFERENCES

[1] S.-J. Chung, A. A. Paranjape, P. Dames, S. Shen, and V. Kumar, "A survey on aerial swarm robotics," *IEEE Trans. Robot.*, vol. 34, no. 4, pp. 837–855, Aug. 2018.

[2] G. Cai, J. Dias, and L. Seneviratne, "A survey of small-scale unmanned aerial vehicles: Recent advances and future development trends," *Unmanned Syst.*, vol. 2, no. 2, pp. 175–199, 2014.

[3] P. Boccardo, F. Chiabrando, F. Dutto, F. G. Tonolo, and A. Lingua, "UAV deployment exercise for mapping purposes: Evaluation of emergency response applications," *Sensors (Switzerland)*, vol. 15, no. 7, pp. 15717–15737, 2015.

[4] C. J. O. Salaan et al., "Close visual bridge inspection using a UAV with a passive rotating spherical shell," *J. Field Robot.*, vol. 35, no. 6, pp. 850–867, 2018.

[5] G. Loianno and V. Kumar, "Cooperative transportation using small quadrotors using monocular vision and inertial sensing," *IEEE Robot. Autom. Lett.*, vol. 3, no. 2, pp. 680–687, Apr. 2018.

[6] A. Ollero et al., "The AEROARMS project: Aerial robots with advanced manipulation capabilities for inspection and maintenance," *IEEE Robot. Autom. Mag.*, vol. 25, no. 4, pp. 12–23, Dec. 2018.

[7] M. Kamel et al., "The Voliro omniorientational hexacopter: An agile and maneuverable tiltable-rotor aerial vehicle," *IEEE Robot. Autom. Mag.*, vol. 25, no. 4, pp. 34–44, Dec. 2018.

[8] M. Tognon and A. Franchi, "Omnidirectional aerial vehicles with unidirectional thrusters: Analysis, optimal design, and motion control," *IEEE Robot. Autom. Lett.*, vol. 3, no. 3, pp. 2277–2282, Jul. 2018.

[9] M. J. Gerber and T.-C. Tsao, "Twisting and tilting rotors for high-efficiency, thrust-vectored quadrotors," *J. Mech. Robot.*, vol. 10, no. 6, 2018, Art. no. 061013.

[10] A. Prorok, M. A. Hsieh, and V. Kumar, "The impact of diversity on optimal control policies for heterogeneous robot swarms," *IEEE Trans. Robot.*, vol. 33, no. 2, pp. 346–358, Apr. 2017.

[11] Y. Zhang and H. Mehrjerdi, "A survey on multiple unmanned vehicles formation control and coordination: Normal and fault situations," in *Proc. Int. Conf. Unmanned Aircr. Syst.*, 2013, pp. 1087–1096.

[12] A. Franchi and P. R. Giordano, "Online leader selection for improved collective tracking and formation maintenance," *IEEE Trans. Control Netw. Syst.*, vol. 5, no. 1, pp. 3–13, Mar. 2018.

[13] C. W. Reynolds, "Flocks, herds, and schools: A distributed behavioral model," *Comput. Graph.*, vol. 21, no. 4, pp. 25–34, 1987.

[14] R. Olfati-Saber, "Flocking for multi-agent dynamic systems: Algorithms and theory," *IEEE Trans. Autom. Control*, vol. 51, no. 3, pp. 401–420, Mar. 2006.

[15] K. K. Oh, M. C. Park, and H. S. Ahn, "A survey of multi-agent formation control," *Automatica*, vol. 53, pp. 424–440, 2015.

[16] S. Zhao and D. Zelazo, "Bearing rigidity theory and its applications for control and estimation of network systems: Life beyond distance rigidity," *IEEE Control Syst. Mag.*, vol. 39, no. 2, pp. 66–83, Apr. 2019.

[17] T. Eren, "Formation shape control based on bearing rigidity," *Int. J. Control*, vol. 85, no. 9, pp. 1361–1379, 2012.

[18] V. Matellán, "Multi-agent versus multi-robot and other byzantine discussions," *J. Phys. Agents*, vol. 2, no. 1, pp. 1–3, 2008.

[19] J. Hendrickx, B. D. Anderson, J.-C. Delvenne, and V. D. Blondel, "Directed graphs for the analysis of rigidity and persistence in autonomous agent systems," *Int. J. Robust Nonlinear Control*, vol. 17, pp. 960–981, 2007.

[20] L. Krick, M. E. Broucke, and B. A. Francis, "Stabilization of infinitesimally rigid formations of multi-robot networks," in *Proc. IEEE Conf. Decis. Control*, 2008, pp. 477–482.

[21] J. Baillieul and L. McCoy, "The combinatorial graph theory of structured formations," in *Proc. IEEE 46th Conf. Decis. Control*, 2007, pp. 3609–3615.

[22] T. Eren, W. Whiteley, and P. N. Belhumeur, "Using angle of arrival (bearing) information in network localization," in *Proc. IEEE Conf. Decis. Control*, 2006, pp. 4676–4681.

[23] B. D. Anderson, C. Yu, F. Bariš, and J. M. Hendrickx, "Control and information architectures for formations," in *Proc. IEEE Int. Symp. Intell. Control*, 2006, pp. 1127–1138.

[24] D. Zelazo, A. Franchi, and P. R. Giordano, "Rigidity theory in SE (2) for unscaled relative position estimation using only bearing measurements," in *Proc. 13th Eur. Control Conf.*, 2014, pp. 2703–2708.

[25] G. Michieletto and A. Cenedese, "Formation control for fully actuated systems: A quaternion-based bearing rigidity approach," in *Proc. IEEE 18th Europ. Control Conf.*, 2019, pp. 107–112.

[26] L. Chen, M. Cao, and C. Li, "Bearing rigidity and formation stabilization for multiple rigid bodies in SE (3)," *Numer. Algebra, Control Optim.*, vol. 9, no. 3, pp. 257–267, 2019.

[27] B. D. Anderson, C. Yu, B. Fidan, and J. Hendrickx, "Rigid graph control autonomous formations," *IEEE Control Syst. Mag.*, vol. 28, no. 6, pp. 48–63, Dec. 2008.

[28] R. Olfati-Saber and R. M. Murray, "Distributed cooperative control of multiple vehicle formations using structural potential functions," in *Proc. IFAC Triennial World Congr.*, 2002, pp. 495–500.

[29] F. Schiano, A. Franchi, D. Zelazo, and P. Robuffo Giordano, "A rigidity-based de-centralized bearing formation controller for groups of quadrotor UAVs," in *Proc. IEEE Int. Conf. Intell. Robots Syst.*, 2016, pp. 5099–5106.

[30] F. Schiano and R. Tron, "The dynamic bearing observability matrix nonlinear observability and estimation for multi-agent systems," in *Proc. IEEE Int. Conf. Robot. Autom.*, 2018, pp. 3669–3676.

[31] A. Franchi, C. Masone, V. Grabe, M. Ryll, H. H. Bülthoff, and P. R. Giordano, "Modeling and control of UAV bearing formations with bilateral high-level steering," *Int. J. Robot. Res.*, vol. 31, no. 12, pp. 1504–1539, 2012.

[32] F. Schiano and P. R. Giordano, "Bearing rigidity maintenance for formations of quadrotor UAVs," in *Proc. IEEE Int. Conf. Robot. Autom.*, 2017, pp. 1467–1474.

[33] D. Zelazo, A. Franchi, H. H. Bülthoff, and P. Robuffo Giordano, "Decentralized rigidity maintenance control with range measurements for multi-robot systems," *Int. J. Robot. Res.*, vol. 34, no. 1, pp. 105–128, 2015.

[34] R. Tron, L. Carlone, F. Dellaert, and K. Daniilidis, "Rigid components identification and rigidity enforcement in bearing-only localization using the graph cycle basis," in *Proc. IEEE Amer. Control Conf.*, 2015, pp. 3911–3918.

[35] S. Zhao, Z. Sun, D. Zelazo, M. Trinh, and H. Ahn, "Laman graphs are generically bearing rigid in arbitrary dimensions," in *Proc. IEEE 56th Annu. Conf. Decis. Control*, 2017, pp. 3356–3361.

[36] M. Trinh, Q. Tran, and H. Ahn, "Minimal and redundant bearing rigidity: Conditions and applications," *IEEE Trans. Autom. Control*, vol. 65, no. 10, pp. 4186–4200, Oct. 2020.

[37] A. Karimian and R. Tron, "Theory and methods forbearing rigidity recovery," in *Proc. 56th IEEE Annu. Conf. Decis. Control*, 2017, pp. 2228–2235.

[38] J. H. Lopez, L. Cao, and J. M. Schwarz, "Jamming graphs: A local approach to global mechanical rigidity," *Phys. Rev. E. Statist., Nonlinear, Soft Matter Phys.*, vol. 88, no. 6, pp. 1–15, 2013.

[39] A. Nixon and E. Ross, "One brick at a time: A survey of inductive constructions in rigidity theory," in *Rigidity and Symmetry.* Berlin, Germany: Springer, 2014, pp. 303–324.

[40] L. Asimow and B. Roth, "The rigidity of graphs," *Trans. Amer. Math. Soc.*, vol. 245, pp. 171–190, Nov. 1978.

[41] S. Briot and P. Robuffo Giordano, "Physical interpretation of bearing rigidity graphs : Application to mobility and singularity analyses," *J. Mech. Robot.*, vol. 11, no. 3, 2019, Art. no. 031006.

[42] B. Servatius, "The geometry of frameworks: Rigidity, mechanisms and CAD," in *Proc. Geometry Work C. Gorini*, 2000, pp. 81–88.

[43] R. Connelly, "Generic global rigidity," *Discr. Comput. Geometry*, vol. 33, pp. 549–563, 2005.

[44] C. Yu, J. Hendrickx, B. D. Anderson, and V. D. Blondel, "Three and higher dimensional autonomous formations: Rigidity, persistence and structural persistence," *Automatica*, vol. 43, pp. 387–402, 2007.

[45] G. Michieletto, A. Cenedese, and D. Zelazo, "A unified dissertation on bearing rigidity theory," *IEEE Trans. Control Netw. Syst.*, vol. 8, no. 4, pp. 1624–1636, Dec. 2021.

[4] In this article, a singular twist is any unconstrained motion, regardless of persistence.

[46] T. Hamel and R. Mahony, "Visual servoing of an under-actuated dynamic rigid-body system: An image-based approach," *IEEE Trans. Robot. Autom.*, vol. 18, no. 2, pp. 187–198, Apr. 2002.
[47] D. Zelazo, P. R. Giordano, and A. Franchi, "Bearing-only formation control using an SE (2) rigidity theory," in *Proc. IEEE Conf. Decis. Control*, 2015, pp. 6121–6126.
[48] M. H. Trinh, S. Zhao, Z. Sun, D. Zelazo, B. D. Anderson, and H. S. Ahn, "Bearing-based formation control of a group of agents with leader-first follower structure," *IEEE Trans. Autom. Control*, vol. 64, no. 2, pp. 598–613, Feb. 2019.
[49] D. Zelazo, A. Franchi, F. Allgöwer, H. H. Bülthoff, and P. Robuffo Giordano, "Rigidity maintenance control for multi-robot systems," in *Proc. Robot.: Sci. Syst.*, 2012.
[50] R. S. Ball, *Theory of Screws: A. Study in the Dynamics of a Rigid Body.* Dublin, Ireland: Hodges, Foster, & Co., 1876.
[51] X. Kong and C. Gosselin, *Type Synthesis of Parallel Mechanisms*, B. S. Groen, O. Khatib, and F. Groen, Eds., vol. 33. Berlin, Germany: Springer, 2015.
[52] P. Long, W. Khalil, and S. Caro, "Kinematic analysis of lower mobility cooperative arms by screw theory," *Proc. 9th Int. Conf. Informat. Control, Autom. Robot.*, 2012, vol. 2, pp. 280–285.
[53] J. P. Merlet, *Parallel Robots*, 2nd ed. Berlin, Germany: Springer, 2006.
[54] S. Briot, P. Martinet, and V. Rosenzveig, "The hidden robot: An efficient concept contributing to the analysis of the controllability of parallel robots in advanced visual servoing techniques," *IEEE Trans. Robot.*, vol. 31, no. 6, pp. 1337–1352, Dec. 2015.
[55] S. Briot, F. Chaumette, and P. Martinet, "Revisiting the determination of the singularity cases in the visual servoing of image points through the concept of hidden robot," *IEEE Trans. Robot.*, vol. 33, no. 3, pp. 536–546, Jun. 2017.
[56] C. Gosselin and J. Angeles, "Singularity analysis of closed-loop kinematic chains," *IEEE Trans. Robot. Autom.*, vol. 6, no. 3, pp. 281–290, Jun. 1990.
[57] M. Coppola, K. N. McGuire, C. De Wagter, and G. C. de Croon, "A survey on swarming with micro air vehicles: Fundamental challenges and constraints," *Front. Robot. AI*, vol. 7, 2020, Art. no. 18.
[58] M. Slavutin and Y. Reich, "Singularity analysis of some multi-platform mechanisms by decomposition and reciprocality," *Mech. Mach. Theory*, vol. 146, 2020, Art. no. 103735.
[59] U. Borrmann, L. Wang, A. D. Ames, and M. Egerstedt, "Control barrier certificates for safe swarm behavior," *IFAC-PapersOnLine*, vol. 48, no. 27, pp. 68–73, 2015.

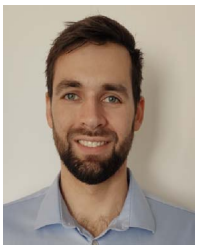

Julian Erskine received the B.Eng. degree in mechanical engineering from Dalhousie University, Halifax, NS, Canada, in 2016 and the M.Sc. degree in robotics from the École Centrale de Nantes, Nantes, France, in 2018, and the Ph.D degree in robotics from the Laboratoire des Sciences de Numerique de Nantes, École Centrale de Nantes, in 2022.

He is currently with a Industry. His research interests are primarily in the domain of aerial robotics, multirobot systems and sensor-based control.

Sébastien Briot received the B.S. and M.S. degrees in mechanical engineering and the Ph.D. degree in robotics from the Institut National des Sciences Appliquées de Rennes, Rennes, France, in 2004 and 2007, respectively.

He was a Postdoctoral Fellow with the Ecole de Technologie Supérieure, Montreal, QC, Canada, in 2008. In 2009, he was with CNRS as a Researcher with the Laboratoire des Sciences du Numérique de Nantes, Nantes, France, where he has been the Head of the ARMEN Research Team since 2017. Since 2022, he has been a CNRS Director of Research in the same lab. He has authored more than 60 referred journal papers, two books, and four inventions. His research interests include the design optimization of robots and the analysis of their performance, especially their singularities.

Dr. Briot was the recipient of the Best Ph.D. Thesis Award in Robotics from the French CNRS in 2007. In 2011, he was also the recipient of two other awards: the Award for the Best Young Researcher from the French Region Bretagne and the Award for the Best Young Researcher from the French Section of the American Society of Mechanical Engineering.

Isabelle Fantoni received the Ph.D. degree, with the European label, in nonlinear control for underactuated mechanical systems from the University of Technology of Compiègne (UTC), Compiègne, France, in 2000.

Between 2001 and 2017, she was a permanent Researcher with Heudiasyc Laboratory, UTC, in Compiègne, France, employed by the French National Foundation for Scientific Research (CNRS) and since 2013, she is the CNRS Research Director. In 2017, she moved to the Laboratory of Digital Sciences of Nantes (LS2N), France, in a team working on Autonomous Robots and Control of Interactions with the Environment (ARMEN team). Her research interests include nonlinear control, modeling and control for Unmanned Aerial Vehicles (UAVs), fault-tolerant control for UAVs, formation control of UAVs, heterogeneous robotic systems in cooperation, control of flying gripper systems, flying parallel robots.

Abdelhamid Chriette received the Industrial Control Engineering degree in study and design of a video acquisition chain from the University of Sidi-Bel-Abbèse, Sidi-Bel-Abbèse, Algeria, in 1997 and the Ph.D. degree in robotics from the Evry-Val-d'Essonne University, Évry-Courcouronnes, France, in 2001.

From 2001 to 2003, he was an "Attaché Temporaire d'Enseignement et de Recherche" with the Evry-Val-d'Essone University. In 2003, he joined the École Centrale de Nantes, Nantes, France, where he is currently an Assistant Professor. He has authored more than 70 papers in all categories (journals/conferences). His research interests include robust sensor-based control for robotic systems, robust nonlinear control, and dynamical modeling of unmanned aerial vehicles.